

1 Large carbon cycle sensitivities to climate across a permafrost thaw gradient in subarctic  
2 Sweden

3  
4 Kuang-Yu Chang\*,  
5 Climate and Ecosystem Sciences Division, Lawrence Berkeley National Laboratory,  
6 Berkeley, California, USA

7 William J. Riley,  
8 Climate and Ecosystem Sciences Division, Lawrence Berkeley National Laboratory,  
9 Berkeley, California, USA

10 Patrick M. Crill,  
11 Department of Geological Sciences, Stockholm University, Stockholm, Sweden

12 Robert F. Grant,  
13 Department of Renewable Resources, University of Alberta, Edmonton, Alberta, Canada

14 Virginia I. Rich,  
15 Department of Microbiology, The Ohio State University, Columbus, Ohio, USA

16 and,  
17 Scott R. Saleska,  
18 Department of Ecology and Evolutionary Biology, University of Arizona, Tucson,  
19 Arizona, USA

20  
21  
22 \*Corresponding author: Kuang-Yu Chang, ckychang@lbl.gov  
23 Climate and Ecosystem Sciences Division, Lawrence Berkeley National Laboratory  
24 Berkeley, California, USA

25 Phone: (510) 495-8141

## Abstract

26  
27 Permafrost peatlands store large amounts of carbon potentially vulnerable to  
28 decomposition. However, the fate of that carbon in a changing climate remains uncertain  
29 in models due to complex interactions among hydrological, biogeochemical, microbial,  
30 and plant processes. In this study, we estimated effects of climate forcing biases present  
31 in global climate reanalysis products on carbon cycle predictions at a thawing permafrost  
32 peatland in subarctic Sweden. The analysis was conducted with a comprehensive  
33 biogeochemical model (*ecosys*) across a permafrost thaw gradient encompassing intact  
34 permafrost palsa with an ice core and a shallow active layer, partly thawed bog with a  
35 deeper active layer and a variable water table, and fen with a water table close to the  
36 surface, each with distinct vegetation and microbiota. Using *in situ* observations to  
37 correct local cold and wet biases found in the Global Soil Wetness Project Phase 3  
38 (GSWP3) climate reanalysis forcing, we demonstrate good model performance by  
39 comparing predicted and observed carbon dioxide (CO<sub>2</sub>) and methane (CH<sub>4</sub>) exchanges,  
40 thaw depth, and water table depth. The simulations driven by the bias-corrected climate  
41 suggest that the three peatland types currently accumulate carbon from the atmosphere,  
42 although the bog and fen sites can have annual positive radiative forcing impacts due to  
43 their higher CH<sub>4</sub> emissions. Our simulations indicate that projected precipitation increases  
44 could accelerate CH<sub>4</sub> emissions from the palsa area, even without further degradation of  
45 palsa permafrost. The GSWP3 cold and wet biases for this site significantly alter  
46 simulation results and lead to erroneous active layer depth (ALD) and carbon budget  
47 estimates. Biases in simulated CO<sub>2</sub> and CH<sub>4</sub> exchanges from biased climate forcing are as  
48 large as those among the thaw stages themselves at a landscape-scale across the

49 examined permafrost thaw gradient. Future studies should thus not only focus on changes  
50 in carbon budget associated with morphological changes in thawing permafrost, but also  
51 recognize the effects of climate forcing uncertainty on carbon cycling.

52 **1. Introduction**

53 Confidence in future climate projections depends on the accuracy of terrestrial  
54 carbon budget estimates, which are presently very uncertain (Friedlingstein et al., 2014;  
55 Arneeth et al., 2017). In addition to the complexity in physical process representations, a  
56 major source of this uncertainty comes from challenges in quantifying climate responses  
57 induced by biogeochemical feedbacks. Increases in atmospheric carbon dioxide (CO<sub>2</sub>)  
58 concentrations can directly stimulate carbon sequestration from plant photosynthesis  
59 (Cox et al., 2000; Friedlingstein et al., 2006) and indirectly stimulate carbon emissions  
60 (e.g., from soil warming and resulting increased respiration), although the predicted  
61 magnitudes of these exchanges strongly depend on model process representations (Zaehle  
62 et al., 2010; Grant, 2013, 2014; Ghimire et al., 2016; Chang et al, 2018).

63 The undecomposed carbon stored in permafrost is of critical importance for  
64 biogeochemical feedbacks to climate because it is about twice as much as currently is in  
65 the atmosphere (Hugelius et al., 2014) and is vulnerable to release to the atmosphere as  
66 permafrost thaws (Schuur et al., 2015). O'Donnell et al. (2012) suggested that permafrost  
67 thaw would result in a net loss of soil organic carbon from the entire peat column because  
68 accumulation rates at the surface were insufficient to balance deep soil organic carbon  
69 losses upon thaw. Jones et al. (2017) indicated that the loss of sporadic and discontinuous  
70 permafrost by 2100 could result in a release of up to 24 Pg of soil carbon from permafrost  
71 peatlands to the atmosphere. Lundin et al. (2016) reported that it is plausible (71%  
72 probability) for the subarctic landscapes to serve as a net carbon source to the atmosphere  
73 while its peatland components being atmospheric carbon sinks, which highlights the  
74 importance of spatial heterogeneity on high latitude carbon budget estimation.

75 In addition to the overall carbon balance of the changing Arctic, the type of  
76 carbon gaseous emission is important to climate feedbacks. High latitudes are predicted  
77 to get wetter (IPCC, 2014), and saturated anaerobic conditions facilitate methane (CH<sub>4</sub>)  
78 production, which is a much more efficient greenhouse gas than CO<sub>2</sub> in terms of global  
79 warming potential. Even habitats that can be net carbon sinks can produce positive  
80 radiative forcing impacts on climate due to CH<sub>4</sub> release, as Bäckstrand et al. (2010)  
81 showed for a subarctic peatland. Under projected warming and wetting trends in the  
82 Arctic (Collins et al., 2013; Bintanja and Andry, 2017), carbon cycle feedbacks over the  
83 permafrost region could become stronger as increased precipitation enhances surface  
84 permafrost thaw and strengthens CH<sub>4</sub> emissions by expansion of anaerobic volume  
85 (Christensen et al., 2004; Wickland et al., 2006).

86 The Stordalen Mire in northern Sweden (68.20°N, 19.03°E) is in the  
87 discontinuous permafrost zone, encompassing a mosaic of thaw stages with associated  
88 distinct hydrology and vegetation (Christensen et al. 2004; Malmer et al., 2005),  
89 microbiota (Mondav and Woodcroft et al., 2014; Mondav et al., 2017; Woodcroft and  
90 Singleton et al., 2018), and organic matter chemistry (Hodgkins et al., 2014). These  
91 landscapes have been shifting over the last half-century to a more thawed state, likely due  
92 to recent warming (Christensen et al. 2004). Drier hummock sites dominated by shrubs  
93 have degraded to wetter sites dominated by graminoids (Malmer et al., 2005; Johansson  
94 et al., 2006). The thaw-induced habitat shifts are associated with increases in landscape-  
95 scale CH<sub>4</sub> emissions (Christensen et al. 2004; Johansson et al., 2006; Cooper et al., 2017)  
96 reflective of the higher CH<sub>4</sub> emissions of the wetter thawed habitats (McCalley et al.,  
97 2014). The higher CO<sub>2</sub> uptake in later thaw-stage habitats has not compensated for the

98 increase in positive radiative forcing from elevated CH<sub>4</sub> emissions (Bäckstrand et al.,  
99 2010; Deng et al., 2014).

100 The impacts of climate sensitivity on the terrestrial carbon cycle have been  
101 investigated at the global scale, and the results highlight the need to consider uncertainty  
102 in climate datasets when evaluating permafrost region carbon cycle simulations  
103 (Ahlström et al., 2017; Guo et al., 2017; Wu et al., 2017). Ahlström et al. (2017) showed  
104 that climate forcing biases are responsible for a considerable fraction (~40%) of the  
105 uncertainty range in ecosystem carbon predictions from 18 Earth System Models (ESMs)  
106 reported by Anav et al. (2013). Guo et al. (2017) concluded that the differences in climate  
107 forcing contribute to significant differences in simulated soil temperature, permafrost  
108 area, and **Active Layer Depth (ALD)**. Wu et al. (2017) demonstrated that differences  
109 among climate forcing datasets contributes more to predictive uncertainty than  
110 differences in apparent model sensitivity to climate forcing. However, notably, none of  
111 these studies accessed the effects on CH<sub>4</sub> emissions, and their spatial resolution could not  
112 represent site-level spatial heterogeneity observed in arctic tundra (Grant et al. 2017a;  
113 2017b).

114 Here, we use the ecosystem model *ecosys*, which employs a comprehensive set of  
115 coupled biogeochemical and hydrological processes, to estimate the effects of climate  
116 forcing uncertainty and sensitivity on CO<sub>2</sub> and CH<sub>4</sub> exchanges and **thaw depth**  
117 simulations. For the Stordalen Mire site, we estimated bias in the Global Soil Wetness  
118 Project Phase 3 (GSWP3) climate reanalysis dataset using site-level long-term  
119 meteorological measurements and evaluated impacts on simulated soil and plant  
120 processes across the permafrost thaw gradient. This approach enables us to assess model

121 sensitivity to individual climate forcing biases, instead of the aggregated uncertainty  
122 range embedded in climate datasets (e.g., variations of climate conditions represented in  
123 different climate datasets) presented in previous studies. We address the following  
124 questions for our study site at the Stordalen Mire: (1) What are the biases embedded in  
125 the GSWP3 climate reanalysis dataset? (2) How do those biases affect model predictions  
126 of thaw depth, CO<sub>2</sub> exchanges, and CH<sub>4</sub> exchanges? (3) How does climate sensitivity  
127 vary across the stages of permafrost thaw? In addition to improving understanding of  
128 permafrost responses to climate, we identify ecosystem carbon prediction uncertainty  
129 induced by climate forcing uncertainty in general as the biases found in GSWP3 were  
130 consistent with other climate reanalysis datasets during the last decade (section 3).

131

## 132 **2. Methods and Data**

### 133 **2.1 Study site description**

134 Our study sites are located at the Stordalen Mire (68.20 °N, 19.03 °E: 351 m  
135 above sea level), which is about 10 km southeast of the Abisko Scientific Research  
136 Station (ANS) in northern Sweden. The Stordalen Mire is in the discontinuous permafrost  
137 zone along the 0 °C isotherm where permafrost at low elevations primarily presents in  
138 peatlands, bordered by lakes to the northwest and southeast (Kokfelt et al., 2010). A large  
139 portion of the mire consists of a slightly elevated drained area underlain by permafrost  
140 characterized by a hummocky topography, and the remaining portion is largely lacking  
141 permafrost with fen-like conditions (Johansson et al., 2006). The recent warming (more  
142 than 1 °C) has deepened the mean ALD measured at the Stordalen Mire by around 20 cm  
143 since the early 1980's, accompanied by palsa collapses and thermokarst erosion



144 (Christensen et al., 2004; Malmer et al., 2005; Johansson et al., 2006). Specifically, the  
145 mean ALD has increased from 0.48 m to 0.63 m in the drier part of the mire and from  
146 0.63 m to 0.86 m in the wetter part, from 1970's to 2000's (Rydén B. E. and Kostov ;  
147 Johansson et al., 2006).

148 Significant changes in climate over this region have been recorded during the last  
149 few decades. The annual mean air temperature measured at the ANS has risen by 2.5 °C  
150 from 1913 to 2006, where it exceeded the 0 °C threshold (0.6 °C in 2006) for the first  
151 time over the past century (Callaghan et al., 2010). The measured annual total  
152 precipitation has also increased from 306 mm y<sup>-1</sup> (years 1913 to 2009) to 336 mm y<sup>-1</sup>  
153 (years 1980 to 2009) (Olefeldt and Roulet, 2012), along with increased variability in  
154 extreme precipitation (Callaghan et al., 2010). The measured annual maximum snow  
155 depth has increased from 59 cm (years 1957 to 1971) to 70 cm (years 1986 to 2000),  
156 however, the snow cover period with snow depth greater than 20 cm has decreased from  
157 5.8 months (years 1957 to 1971) to 4.9 months (years 1986 to 2000) (Malmer et al.,  
158 2005).

159 Inception of peat deposition at the Stordalen Mire has been dated at around 6,000  
160 calendar years before present (cal. BP) (Sonesson 1972) in the southern part of the mire  
161 and at around 4,700 cal. BP in the northern part (Kokfelt et al., 2010). Kokfelt et al.  
162 (2010) suggested that permafrost aggregation initiated during the Little Ice Age (around  
163 120–400 cal. BP) in the Stordalen Mire. At present, the Stordalen Mire can be broadly  
164 classified into three peatland types: intact permafrost palsa, partly thawed bog, and fen  
165 (Hodgkins et al., 2014), hereafter referred to as palsa, bog, and fen (Figure 1). The spatial  
166 distribution of these peatland types in 2000 are described in Olefeldt and Roulet (2012).

167 Based on Swedish military photography, all three of the investigated peatland  
168 types have existed since at least the 1930's. The palsa sites are ombrotrophic and raised  
169 0.5 to 2.0 m above their surroundings, with a relatively thin peat layer (0.4 to 0.7 m,  
170 Rydén et al., 1980), thinner active layer depth (less than 0.7 m in late summer), and no  
171 measurable water table depth (Bäckstrand et al., 2008a; 2008b; Olefeldt and Roulet,  
172 2012). The bog sites are ombrotrophic and are wetter than the palsa sites, with a thicker  
173 peat layer (0.5 to ~1 m, Rydén et al., 1980), deeper ALD (greater than 0.9 m, the deepest  
174 measurement depth), and water table depth fluctuating from 35 cm below the peat surface  
175 to the ground surface (Bäckstrand et al., 2008a; 2008b; Olefeldt and Roulet, 2012). The  
176 fen sites are minerotrophic, receiving a large amount of water from a lake to the east of  
177 the mire, with water table depths near or above the ground surface (Bäckstrand et al.,  
178 2008a; 2008b; Olefeldt and Roulet, 2012).

179 Differences in hydrology and permafrost conditions create high spatial  
180 heterogeneity with different soil moisture, pH, and nutrient conditions that support  
181 different plant communities (Bäckstrand et al., 2008a; 2008b). The palsa is dominated by  
182 dwarf shrubs with some sedges, feather mosses, and lichens (Malmer et al., 2005;  
183 Bäckstrand et al., 2008a; 2008b; Olefeldt and Roulet, 2012). The bog is dominated by  
184 *Sphagnum* spp. mosses with a moderate abundance of sedges (Malmer et al., 2005;  
185 Bäckstrand et al., 2008a; 2008b; Olefeldt and Roulet, 2012). The fen sites we studied are  
186 dominated by sedges (Bäckstrand et al., 2008a; 2008b).

187

## 188 2.2 Field measurements

189 Continuous daily meteorological measurements have been recorded at the ANS  
190 since 1913, including air temperature, precipitation, wind speed, wind direction, relative  
191 humidity, and snow depth. Measurements of solar radiation, longwave radiation, and soil  
192 temperature are also available at the ANS since 1982. The soil thaw depth (measured to  
193 90 cm) and water table depth measurements were taken in the three peatland types 3 to 5  
194 times per week from early May to mid-October during 2003 to 2007 (Bäckstrand et al.,  
195 2008b).

196 CO<sub>2</sub> and CH<sub>4</sub> exchanges at the three peatland types were measured with  
197 automated chambers during the thawed seasons from 2002 to 2007 (Bäckstrand et al.,  
198 2008b). Chamber lids were removed when snow accumulates in winter (around  
199 November), and the sampling periods for each year ranged from 60 days (28 March (day  
200 87) to 27 May (day 147)) in 2002 (shortest) to 193 days (28 May (day 148) to 7  
201 December (day 341)) (longest) (Bäckstrand et al., 2008b; Bäckstrand et al., 2010). Three  
202 chambers were installed in the palsa, another three in the bog, and two more in the fen  
203 (we term each chamber a 'subsite' in the following). Each chamber covered an area of  
204 0.14 m<sup>2</sup> with a height of 25–45 cm depending on the vegetation and the depth of insertion  
205 and was closed for 5 minutes every 3 hours to measure CO<sub>2</sub> and total hydrocarbon (THC)  
206 exchanges. CH<sub>4</sub> exchanges were manually observed approximately 3 times per week, and  
207 these measurements were used to quantify the proportion of CH<sub>4</sub> in the measured THC  
208 (Bäckstrand et al., 2008a). The CH<sub>4</sub> exchanges were near zero in the palsa sites  
209 (Bäckstrand et al., 2008a; Bäckstrand et al., 2008b; Bäckstrand et al., 2010), so they were  
210 not used in model evaluation. We used the CO<sub>2</sub> and CH<sub>4</sub> exchanges observed at 3-hourly  
211 steps when the R<sup>2</sup> values recorded in the measurements were greater than 0.8 (Tokida et

212 al., 2007), and then calculated the associated daily mean exchanges when there were 8  
213 measurements per day (Table 1). The quality-controlled daily measurements only  
214 covered 12.4–33.7% of the daily data points because of the lack of continuous quality-  
215 controlled 3-hourly measurements. The data screening was applied to exclude unreliable  
216 measurements and avoid biases from inappropriate gap filling, which is necessary for  
217 model evaluations. More detailed descriptions of the CO<sub>2</sub> and CH<sub>4</sub> exchanges  
218 measurements can be found in Bäckstrand et al. (2008a).

219

### 220 **2.3 GSWP3**

221 GSWP3 is an ongoing modeling activity that provides global gridded  
222 meteorological forcing (0.5° x 0.5° resolution) and investigates changes in energy, water,  
223 and carbon cycles throughout the 20<sup>th</sup> and 21<sup>st</sup> centuries. The GSWP3 dataset is based on  
224 the 20<sup>th</sup> Century Reanalysis (Compo et al., 2011), using a spectral nudging dynamical  
225 downscaling technique described in Yoshimura and Kanamitsu (2008). A more detailed  
226 description of the GSWP can be found in Dirmeyer (2011) and van den Hurk et al.  
227 (2016).

228 In this study, we extracted the meteorological conditions at the Stordalen Mire  
229 from 1901 to 2010 from the GSWP3 climate reanalysis dataset. The 3-hourly products of  
230 air temperature, precipitation, solar radiation, wind speed, and specific humidity were  
231 interpolated to hourly intervals with cubic spline interpolation to serve as the  
232 meteorological inputs used in our model.

233 The GSWP3 dataset was chosen over other existing climate reanalysis datasets for  
234 its spatial and temporal resolutions. For example, the Climatic Research Unit (CRU;

235 Harris et al., 2014) dataset provided monthly meteorological forcing at 0.5° x 0.5°  
236 resolution; the National Centers for Environmental Prediction (NCEP; Kalnay et al.,  
237 1996; Kanamitsu et al., 2002) dataset provided 6-hourly meteorological forcing at T62  
238 Gaussian grid (~1.915° x 1.895° resolution); the CRUNCEP (Viovy, 2018) dataset  
239 provided 6-hourly meteorological forcing at 0.5° x 0.5° resolution; and the European  
240 Centre for Medium-Range Weather Forecasts (ECMWF; Berrisford et al., 2011) dataset  
241 provided 3-hourly meteorological forcing with 125 km (~1.125°) horizontal resolution.

242

## 243 **2.4 Model description**

244 *Ecosys* is a comprehensive biogeochemistry model that simulates ecosystem  
245 responses to diverse environmental conditions with explicit representations of microbial  
246 dynamics and soil carbon, nitrogen, and phosphorus biogeochemistry. The above-ground  
247 processes are represented in multi-layer plant interacting canopies that are allowed to  
248 change with changing environmental conditions, and the below-ground processes are  
249 represented in multiple soil layers with multi-phase subsurface reactive transport. *Ecosys*  
250 operates at variable time steps (down to seconds) determined by convergence criteria, and  
251 it can be applied at patch scale (spatially homogenous one-dimensional) and landscape  
252 scale (spatially variable two- or three-dimensional). Detailed descriptions, including  
253 inputs, outputs, governing equations, parameters, and references of the *ecosys* model can  
254 be found in Grant (2013). A qualitative summary of the *ecosys* model structure is  
255 provided in the supplemental material to this article.

256 The *ecosys* model has been extensively tested against eddy covariance fluxes and  
257 related ecophysiological measurements with a wide range of sites and weather conditions

258 in boreal, temperate, and tropical forests (Grant et al., 2007a; Grant et al., 2007c; Grant et  
259 al., 2009a; Grant et al., 2009b; Grant et al., 2009c; Grant et al., 2010), wetlands (Dimitrov  
260 et al., 2011; Grant et al., 2012b; Dimitrov et al., 2014; Mezbahuddin et al., 2014),  
261 grasslands (Grant and Flanagan, 2007; Grant et al., 2012a), tundra (Grant et al., 2003;  
262 Grant et al., 2011b; Grant 2015; Grant et al., 2015), croplands (Grant et al., 2007b; Grant  
263 et al., 2011a), and other permafrost-associated habitats (Grant and Roulet, 2002; Grant,  
264 2017a; Grant et al., 2017b). All *ecosys* model structures are unchanged from those  
265 described in these earlier studies.

## 266 **2.5 Experimental design**

267 To evaluate the effects of climate on model predictions, we conducted four sets of  
268 simulations at each of the three peatland types at the Stordalen Mire from 1901 to 2010.  
269 The climate data from 1901 to 2001 were used for model initialization (i.e., spinup) and  
270 those from 2002 to 2010 were used for analysis. The 110 year simulations were  
271 performed to ensure the simulation was equilibrated with local climate (Grant et al.  
272 2017a).

273 The meteorological conditions for all the simulations were based on the hourly  
274 data extracted from the GSWP3 climate reanalysis dataset (section 2.3). The monthly  
275 mean bias of the GSWP3 for this location was calculated by comparing it to the air  
276 temperature and precipitation measured at the ANS, for years 1913 to 2010 (section 3.1).  
277 The full series of air temperature and precipitation extracted from GSWP3 were then  
278 bias-corrected using the monthly mean bias calculated from 1913 to 2010; we label this  
279 model scenario CTRL. Our bias correction was conceptually similar to the one used in  
280 Ahlström et al. (2017), where the bias-corrected climate forcing fields were the ESM

281 outputs adjusted by the corresponding bias calculated from observations in a reference  
282 period.

283         The simulation results from CTRL should represent the reliability of applying  
284 *ecosys* at the Stordalen Mire because CTRL is driven by the best local climate  
285 description. We first evaluated predicted thaw depth, water table depth, and CO<sub>2</sub> and CH<sub>4</sub>  
286 exchanges using the CTRL simulation (section 3.2 to 3.4). In the second set of  
287 simulations, BIASED-COLD, the biased GSWP3 air temperature data was used, and we  
288 corrected only the GSWP3 precipitation. Deviations between CTRL and BIASED-COLD  
289 reflect biased air temperature's effects on responses across the thaw gradient. In the third  
290 set of simulations, BIASED-WET, we bias-corrected the air temperature extracted from  
291 GSWP3, which allows us to quantify the effects of biased precipitation. Finally, we used  
292 the meteorological conditions directly extracted from GSWP3 to drive our fourth set of  
293 simulations, BIASED-COLD&BIASED-WET, which reveals the uncertainty range of  
294 subarctic peatland simulation associated with the local biases in GSWP3 climate forcing.

295         While the three peatland types share the same climate conditions, they differ in  
296 soil hydrologic conditions and vegetation characteristics (section 2.1; Figure 1). The bulk  
297 density and porosity profiles were set to the values reported in Rydén et al. (1980), who  
298 suggested a decreasing trend of bulk density and an increasing trend of porosity from  
299 *palsa* (0.12 Mgm<sup>-3</sup> at surface; 92–93% within the upper 10 cm) to bog and fen (0.06  
300 Mgm<sup>-3</sup> at surface; 96–97% within the upper 10 cm). The peatland soil carbon-to-nitrogen  
301 (CN) ratios and pH values were assigned according to Hodgkins et al. (2014), who  
302 documented an increasing trend of pH from *palsa* (4.0), to bog (4.2), to fen (5.7), and a  
303 decreasing trend of soil organic matter CN ratio from bog (46±18), to *palsa* (39±24), to

304 fen ( $19 \pm 0.4$ ). Common values of field capacity (0.4) and wilting point (0.15) were used  
305 for the three peatland types (Deng et al., 2014). The soil property and vegetation  
306 parameters used in our simulation for the three peatland types are summarized in  
307 Supplemental Material Table1 and Supplemental Material Table2, respectively.

308

### 309 **3 Results and Discussion**

#### 310 **3.1 GSWP3 climate comparison to observations**

311 As described in section 2.3, we extracted meteorological conditions at the  
312 Stordalen Mire from the GSWP3 climate reanalysis dataset. The closest GSWP3 grid cell  
313 was centered at  $68.0^\circ\text{N}$  and  $19.0^\circ\text{E}$ , which covers the Stordalen Mire and the ANS. The  
314 annual mean air temperature and precipitation calculated at this GSWP3 grid cell were -  
315  $3.65^\circ\text{C}$  and  $683.88 \text{ mm y}^{-1}$ , respectively, for years 1913 to 2010. A cold bias ( $-3.09^\circ\text{C}$ )  
316 was identified in the GSWP3 annual mean air temperature during the 1913 to 2010  
317 period, although a very high correlation coefficient ( $r = 0.99$ ) was found when compared  
318 with the ANS measurements (Figure 2a). Both time series exhibit an overall warming  
319 trend from the early 20<sup>th</sup> century to the present ( $0.01^\circ\text{C y}^{-1}$ ), with an even larger warming  
320 trend from 1980 to 2010 ( $0.05^\circ\text{C y}^{-1}$  [ANS] and  $0.04^\circ\text{C y}^{-1}$  [GSWP3]).

321 Similarly, the GSWP3 annual total precipitation data correlates well with ANS  
322 measurements ( $r = 0.80$ ) but has a wet bias of  $380 \text{ mm y}^{-1}$  between 1913 and 2010  
323 (Figure 2b). An increasing trend in annual total precipitation was recorded in both time  
324 series from the early 20<sup>th</sup> century to present ( $0.47 \text{ mm y}^{-2}$  [ANS] and  $1.07 \text{ mm y}^{-2}$   
325 [GSWP3]), although a decreasing trend was found from 1980 to 2010 ( $-0.56 \text{ mm y}^{-2}$   
326 [ANS] and  $-2.39 \text{ mm y}^{-2}$  [GSWP3]).



327 The seasonal cycle of the GSWP3 monthly mean air temperature also matches  
328 that measured at the ANS, with a very high correlation coefficient ( $r = 0.99$ ; Figure 3a).  
329 The underestimation bias and inter-annual variability of GSWP3 air temperature are  
330 greater in winter (maximum underestimate in December, at  $-4.52\text{ }^{\circ}\text{C}$  with inter-annual  
331 variability of  $3.53\text{ }^{\circ}\text{C}$ ) and smaller in summer (minimum underestimate in July, at  $-1.52$   
332  $^{\circ}\text{C}$  with inter-annual variability of  $1.65\text{ }^{\circ}\text{C}$ ), respectively.

333 The magnitude and inter-annual variability of the GSWP3 monthly mean  
334 precipitation are comparable between winter and summer, while the ANS measurements  
335 exhibit stronger seasonality with lower magnitudes during winter. Despite the differences  
336 found in seasonal patterns, a high correlation coefficient ( $r = 0.64$ ) was found between the  
337 monthly mean precipitation extracted from GSWP3 and the ANS measurements. The  
338 overestimation of monthly mean precipitation was greatest in December ( $43.25\text{ mm}$   
339  $\text{month}^{-1}$ ) and smallest in August ( $18.75\text{ mm month}^{-1}$ ).

340 These comparisons suggest that GSWP3 air temperature and precipitation data  
341 reasonably capture measured seasonal and long-term trends over past decades, but are  
342 biased cold and wet compared to observations, especially during winter. Similar cold and  
343 wet biases exist in CRUNCEP and ECMWF climate reanalysis datasets during our 2003  
344 to 2007 study period (Supplemental Material Figure 1). The annual mean air temperature  
345 and precipitation at the Stordalen Mire for years 2003 to 2007 were  $-2.49\text{ }^{\circ}\text{C}$  and  $795.09$   
346  $\text{mm y}^{-1}$ ;  $-2.46\text{ }^{\circ}\text{C}$  and  $708.60\text{ mm y}^{-1}$ ; and  $-2.28\text{ }^{\circ}\text{C}$  and  $765.67\text{ mm y}^{-1}$  in the GSWP3,  
347 CRUNCEP, and ECMWF climate reanalysis datasets, respectively.

348

### 349 **3.2 Model testing**

### 350 3.2.1 Thaw depth

351 We first evaluated *ecosys* against observations using bias-corrected climate  
352 forcing (i.e., the CTRL simulation). Predicted thaw depth agrees well with measurements  
353 collected from 2003 to 2007 for all examined peatland types (Figure 4), with a correlation  
354 coefficient of 0.95, 0.87, and 0.41 at the palsa, bog, and fen, respectively. Both  
355 simulations and observations show that the rate of thaw depth deepening in the summer  
356 varies with peatland type (i.e., relatively slow, moderate, and rapid in the palsa, bog, and  
357 fen, respectively).

358 Predicted and observed maximum thaw depths (i.e., ALD) in the intact permafrost  
359 palsa were between 45 and 60 cm in September. In the partly thawed bog, the simulated  
360 thaw depth is slightly shallower than that observed before August. The simulated bog  
361 thaw depth exceeds 90 cm by the end of August, which matches the time when measured  
362 thaw depth reaches its maximum. In contrast, the thaw depth exceeds 90 cm nearly one  
363 month earlier in the fen. The patterns of thawing permafrost presented here are consistent  
364 with Deng et al. (2014), who simulated the same site using the DNDC model.

365

### 366 3.2.2 CO<sub>2</sub> exchanges

367 The daily Net Ecosystem Exchange (NEE) simulated in the CTRL simulation  
368 reasonably captures observed seasonal dynamics from 2003 to 2007 for all the examined  
369 peatland types (Figure 5). The simulations and observations generally showed net CO<sub>2</sub>  
370 uptake (with some episodic CO<sub>2</sub> emissions) during summer and release during winter.  
371 The observations and simulations also showed large CO<sub>2</sub> emissions in the palsa site  
372 during fall of 2004. Simulated fall CO<sub>2</sub> bursts in the three sites in other years could not be

373 confirmed because of a lack of observations during these periods. Similar to the patterns  
374 reported in Raz-Yaseef et al. (2016), some episodic CO<sub>2</sub> emission pulses were simulated  
375 as surface ice thaws in spring, but there were no measurements to confirm those events.  
376 The correlation coefficients of the simulated and observed daily NEE ranged from 0.58 to  
377 0.60, and most of the discrepancies between the simulations and observations were within  
378 the ranges of NEE variability measured at different subsites (automated chambers) within  
379 the same peatland type. The simulated CO<sub>2</sub> uptake rates in the bog were greater than the  
380 observations in summer, which could be due to overestimated plant biomass or  
381 overestimated CO<sub>2</sub> uptake rate per plant biomass. However, we currently do not have  
382 data to examine the cause of this overestimation because the CO<sub>2</sub> flux derived from  
383 automated chambers only represents the aggregated results of all controlling factors.

384 As described in section 2.2, simulated CO<sub>2</sub> exchanges were evaluated for 3-hourly  
385 and daily time steps when quality-controlled measurements were available (R<sup>2</sup> values and  
386 relative root mean squared errors (RRMSEs) shown in Table 2). Simulated NEE is in  
387 reasonable agreement with the 3-hourly NEE measurements with RRMSEs ranging  
388 from 8.4 to 19.1%. Model comparisons with observations were generally poorer at daily  
389 time steps, although the calculated RRMSEs were comparable to those reported in Deng  
390 et al. (2014). We suspect these differences resulted from uncertainty in determining an  
391 accurate observed daily NEE that is representative of the entire peatland type. This may  
392 be due to (1) limited daily data points (less than 14% across the study period, Table 1)  
393 due to lack of continuous quality-controlled 3-hourly measurements, and (2) the large  
394 variability of daily NEE ranges measured at different subsites within the same peatland  
395 type (Figure 5). Our results thus indicate that NEE is affected by thaw stage (Bäckstrand

396 et al., 2010; Deng et al., 2014) and fine scale spatial heterogeneity of the system. More  
397 detailed measurements with higher spatial and temporal resolutions within the same  
398 peatland type would be necessary to characterize the effects of this type of heterogeneity.

399

### 400 3.2.3 Water table depth and CH<sub>4</sub> exchanges

401 Simulated water table depth generally captures observed seasonal patterns  
402 measured in the bog and fen sites from 2003 to 2007 (Figure 6a, c). During summer, the  
403 predicted bog water table depth fluctuates around the ground surface (-7 to -1 cm), and  
404 the predicted water table depth is at or above the ground surface in the fen. Water table  
405 depths simulated by *ecosys* are generally higher than measured in the bog, where  
406 measured water table depths are often below the ground surface with greater seasonal  
407 variability. Simulated fen water table depths have better overall fit to observations, being  
408 higher (~5 cm) than measurements in 2003 and 2004, close to measurements in 2005 and  
409 2006, and slightly deeper (~2 cm) than measurements in 2007. These differences in  
410 modeled and observed water table depth could be driven by the limitations of our one-  
411 dimensional column simulation that could not resolve topographic effects and thus hinder  
412 the variations of water table depth, which is a particular issue in simulating the dynamic  
413 water table of the bog. For example, no excessive water could be transported to the  
414 neighboring grids to deepen local water table depth under our current model  
415 configuration. A multi-dimensional simulation that includes realistic topographic effects  
416 could help improve the representation of water table dynamics, and estimates of the  
417 measurement uncertainty would help facilitate the assessment of simulation bias.

418 Simulated and measured daily CH<sub>4</sub> exchanges correlate reasonably well in the  
419 bog ( $r = 0.49$ ) and well in the fen ( $r = 0.65$ ) across the study period (Figure 6b, d). Both  
420 the simulations and observations have stronger CH<sub>4</sub> emissions during summer with peak  
421 emissions in late summer. Some episodic CH<sub>4</sub> emission pulses (Mastepanov et al., 2008)  
422 were simulated during shoulder seasons, and the simulated amount of post-growing  
423 season CH<sub>4</sub> emissions agrees well with those measured in 2007.

424 Most of the discrepancies between simulated and observed CH<sub>4</sub> emissions were  
425 within the variability of measurements across subsites within the same peatland type. The  
426 3-hourly and daily RRMSEs ranged from 11.1 to 22.3% (Table 2) and the daily RRMSEs  
427 were comparable to results presented in Deng et al. (2014). Our results show that model  
428 evaluation of CH<sub>4</sub> emissions with finer temporal resolution observations is not necessarily  
429 superior to evaluation with coarser temporal resolution, as compared to the NEE  
430 counterpart, which could be related to comparatively lesser CH<sub>4</sub> emission variability  
431 measured across subsites within the same peatland type (Figure 6b, d).

432

### 433 3.3 Variability across the permafrost thaw gradient

434 Thaw rate and ALD increase along the thaw gradient (i.e., palsa to bog to fen),  
435 and landscape variations are generally greater than simulated inter-annual variability  
436 (Figure 7a). Maximum carbon uptake also increases along the thaw gradient, and  
437 variations across the landscape are comparable with simulated intra-seasonal and inter-  
438 annual variabilities (Figure 7b). The simulated mean seasonal cumulative NEE were  
439 calculated based on the seasonality identified in Bäckstrand et al. (2010) to help facilitate  
440 the inter-comparison of carbon budgets estimated at the Stordalen Mire, and to better

441 capture the actual seasonality recorded at the study site. The results show that the  
442 magnitude of mean growing season CO<sub>2</sub> uptake is highest in the fen and lowest in the  
443 palsa (Table 3). The same rank applies to the magnitude of mean CO<sub>2</sub> emissions over the  
444 non-growing season, although differences across the thaw gradient are smaller.

445 CH<sub>4</sub> emission rates increase significantly along the thaw gradient, and the palsa  
446 site emissions are negligible (Figure 7c). Mean cumulative CH<sub>4</sub> emissions simulated in  
447 the fen are much higher than those in the bog, and most CH<sub>4</sub> emissions occur during the  
448 growing season (Table 3). The higher CH<sub>4</sub> emissions in the fen can be attributed to its  
449 faster seasonal thaw rate (Figure 7a) and a water table depth close to the surface (Figure  
450 6c). Seasonal cumulative NEE and CH<sub>4</sub> emissions from observations could not be  
451 accessed due to the lack of continuous quality controlled carbon flux measurements  
452 during our study period (Table 1).

453

### 454 **3.4 Climate sensitivity of permafrost thaw**

#### 455 **3.4.1 Thaw responses to climate**

456 Our results indicate that the ALD currently simulated in the bog and fen is around  
457 108 cm and 130 cm, respectively. However, the maximum depth of our thaw depth  
458 measurements is 90 cm, which makes it difficult to evaluate our model performance on  
459 ALD simulation. Our results highlight the need to acquire measurements at deeper depth  
460 to resolve whether there is no permafrost currently remaining in the bog and fen, or there  
461 is a talik with permafrost developed deeper than the simulated ALDs. Such information  
462 could be important in predicting microbial activity and thermokarst in permafrost

463 peatlands (Schuur et al., 2015), but it may not significantly alter the effects of climate  
464 forcing uncertainty discussed in our study.

465 For each of the four sets of simulations with different climate forcing (section  
466 2.5), simulated mean ALD from 2003 to 2007 is always greatest in the fen and lowest in  
467 the palsa (Figure 8). This consistent trend along the thaw gradient indicates that ALDs  
468 are largely regulated by their distinct ecological and hydrological conditions, because all  
469 three sites had the same climate forcing in each set of simulations (i.e., CTRL, BIASED-  
470 COLD, BIASED-WET, and BIASED-COLD&BIASED-WET). Therefore, the palsa,  
471 bog, and fen have different resilience against the changes in climate forcing, and this type  
472 of ecosystem resilience plays an important role in determining ALD under changes in  
473 climate conditions.

474 Effects of climate on simulated ALD are similar across peatland types (Figure 8).  
475 With increased precipitation (BIASED-WET vs. CTRL), simulated ALD generally  
476 becomes deeper with greater inter-annual variability because the increased snowpack  
477 depth keeps the soil warmer with lower soil ice content during winter. This effect is less  
478 prominent in the comparison between experiments BIASED-COLD and BIASED-  
479 COLD&BIASED-WET, because the cold biases in these two experiments (section 3.1)  
480 constrain thaw depth development. For example, summertime soil heating in some of the  
481 simulation years was not strong enough to thaw the soil ice between 20-40 cm completely  
482 in the BIASED-COLD&BIASED-WET run, resulting in shallower ALDs simulated in  
483 the palsa and fen even with the snowpack warming effect. The simulated ALD also  
484 becomes deeper with higher air temperature (CTRL vs. BIASED-COLD; BIASED-WET  
485 vs. BIASED-COLD&BIASED-WET) at all the examined peatland types. This response

486 is more evident in the comparison between experiments BIASED-WET and BIASED-  
487 COLD&BIASED-WET, probably driven by their wet biases (section 3.1) that facilitate  
488 thaw depth deepening (via increased thermal conductivity and advective heat transport;  
489 Grant et al. 2017a). Similar dependencies between ALD and climate were shown in  
490 Åkerman and Johansson (2008) and Johansson et al. (2013), based on multi-year  
491 measurements and snow manipulation experiments.

492 Therefore, the combined cold and wet biases in the GSWP3 climate reanalysis  
493 dataset could counteract their individual effects on simulated ALD development at the  
494 Stordalen Mire. Our results indicate a 28.6%, 0.7%, and 11.7% underestimation of ALD  
495 simulated in the palsa, bog, and fen, respectively, when applying the GSWP3 climate  
496 reanalysis data over this region without proper bias correction (BIASED-  
497 COLD&BIASED-WET vs. CTRL). Our sensitivity analysis suggests that projected  
498 warming and wetting trends (Collins et al., 2013) could significantly increase ALD in the  
499 Arctic, since increases in precipitation and air temperature can both contribute to ALD  
500 deepening.

501

### 502 **3.4.2 Carbon budget responses to climate**

503 Simulations with the four climate forcing datasets (section 2.5) indicate annual  
504 mean (from 2003 to 2007) CO<sub>2</sub> sinks and CH<sub>4</sub> sources, except the weak CO<sub>2</sub> emissions  
505 simulated in the fen in experiment BIASED-COLD&BIASED-WET due to reduced  
506 sedge productivity driven by increased temperature and oxygen stresses (Figure 9a,b).  
507 Our results also indicate that differences in annual CO<sub>2</sub> and CH<sub>4</sub> exchanges across the  
508 four climate forcing datasets for a single peatland type are as large as those across



509 peatland types for a single climate forcing dataset (Figure 9a,b). These large CO<sub>2</sub> and  
510 CH<sub>4</sub> exchanges climate sensitivities demonstrate that the peatland's dynamical responses  
511 to climate have stronger effects on the carbon cycle than on ALDs (Figure 8).

512 With bias-corrected precipitation, increased air temperature (CTRL vs. BIASED-  
513 COLD) leads to stronger CO<sub>2</sub> uptake and greater CH<sub>4</sub> emissions at all the examined  
514 peatland types (Figure 9a,b), mainly because enhanced sedge growth facilitates carbon  
515 cycling under a warmer environment (results not shown). This air temperature sensitivity  
516 affects CO<sub>2</sub> and CH<sub>4</sub> exchanges within the same peatland type without significantly  
517 changing ALD (Figure 8). For both experiments, CO<sub>2</sub> uptake and CH<sub>4</sub> emissions are  
518 greatest in the fen and lowest in the palsa, consistent with the measurements reported in  
519 Bäckstrand et al. (2010) for the same period. Based on the Coupled Model  
520 Intercomparison Project, phase 5 (CMIP5) ESM simulations, arctic annual mean surface  
521 air temperature is projected to increase by 8.5±2.1 °C over the 21<sup>st</sup> century (Bintanja and  
522 Andry, 2017). This projected air temperature increase is more than double the air  
523 temperature difference between site-observed and GSWP3 temperatures, which could  
524 significantly enhance CH<sub>4</sub> emissions regardless of palsa degradation into bog and fen.

525 On the other hand, wet biases (BIASED-WET and BIASED-COLD&BIASED-  
526 WET) increase CH<sub>4</sub> emissions in the palsa; wetter and colder conditions result in as much  
527 CH<sub>4</sub> release as the current fen, while wetter conditions alone drive palsa emissions  
528 comparable to the current bog (Figure 9b). The large precipitation sensitivity found in  
529 palsa CH<sub>4</sub> emissions could have strong effects on palsa carbon cycling because arctic  
530 precipitation is projected to increase by 50 – 60% towards the end of the 21<sup>st</sup> century  
531 (based on CMIP5 estimates; Bintanja and Andry, 2017). The comparison between

532 experiments BIASED-WET and BIASED-COLD&BIASED-WET shows that in the  
533 tundra, increased air temperature strengthens CO<sub>2</sub> uptake and weakens CH<sub>4</sub> emissions.  
534 This shift is primarily driven in the model by increased shrub and moss productivity  
535 under the warmer environment, which facilitate CO<sub>2</sub> uptake while drying out the soil and  
536 reducing CH<sub>4</sub> emissions (results not shown). In the bog and fen sites, increased air  
537 temperature under wet bias strengthens both the simulated CO<sub>2</sub> uptake and CH<sub>4</sub>  
538 emissions (BIASED-WET vs. BIASED-COLD&BIASED-WET), due to enhanced sedge  
539 growth under the warmer environment that facilitates carbon cycling in the experiment  
540 BIASED-WET. The low CH<sub>4</sub> emissions in bog and fen simulated in experiment  
541 BIASED-COLD&BIASED-WET are driven by increased temperature and oxygen  
542 stresses that greatly reduce heterotrophic respiration (CH<sub>4</sub> production) and sedge cover  
543 (aerenchyma transport).

544 We assessed the integrated effects of the changes in CO<sub>2</sub> and CH<sub>4</sub> exchanges  
545 identified in the full suite of simulations in terms of the Net Carbon Balance (NCB) and  
546 net emissions of greenhouse gases expressed as CO<sub>2</sub> equivalents (Net Greenhouse Gas  
547 Balance; NGGB). NCB was defined as the sum of the annual total CO<sub>2</sub> and CH<sub>4</sub>  
548 exchanges. NGGB was defined in a similar fashion as the NCB, but considers the greater  
549 radiative forcing potential of CH<sub>4</sub> than CO<sub>2</sub> (28 times over a 100-year horizon, Myhre et  
550 al., 2013) when calculating the annual total. The calculated NCB values are mostly  
551 negative because the stronger CO<sub>2</sub> uptake dominates the weaker CH<sub>4</sub> emissions (Figure  
552 9c). The results suggest that all the examined peatland types serve as net carbon sinks  
553 under current climate (CTRL), consistent with the estimates reported in Deng et al.  
554 (2014) and Lundin et al. (2016). We find a 24, 36, and 38 g C m<sup>-2</sup> y<sup>-1</sup> underestimation of

555 NCB simulated in the palsa, bog, and fen sites, respectively, due to the cold and wet  
556 biases in the GSWP3 climate reanalysis dataset (BIASED-COLD&BIASED-WET vs.  
557 CTRL). NGGB is affected more strongly by CH<sub>4</sub> emissions (Figure 9d) due to its larger  
558 radiative forcing potential. NGGB values are positive over the bog and fen, suggesting  
559 that these sites have positive radiative forcing impacts despite being net carbon sinks.  
560 NGGB simulated in the palsa is generally negative (i.e., a net sink from the atmosphere)  
561 due to lower CH<sub>4</sub> emissions, except for the simulation conducted without any climate bias  
562 correction (correcting only air temperature increased CH<sub>4</sub> emissions but not enough to  
563 compensate for the significantly higher CO<sub>2</sub> sink). Our results indicate that the simulated  
564 NGGB would be biased by 298, -66, and -252 g CO<sub>2</sub>-eq m<sup>-2</sup> y<sup>-1</sup> in the palsa, bog, and fen,  
565 respectively, without proper bias correction for the GSWP3 climate reanalysis dataset  
566 (BIASED-COLD&BIASED-WET vs. CTRL). Using the GSWP3 products directly thus  
567 effectively eliminates the positive radiative forcing from the expanding bog and fen,  
568 while creating a potentially dramatically inaccurate positive radiative forcing from the  
569 shrinking palsa.

570

### 571 **3.4.3 Climate sensitivity versus landscape heterogeneity**

572 Climate sensitivity and landscape heterogeneity are defined here as variability  
573 across the four climate forcing datasets for a single peatland type, and variability across  
574 three peatland types with bias-corrected climate (CTRL), respectively. We estimated  
575 carbon cycle variability associated with climate sensitivity and landscape heterogeneity to  
576 quantify the corresponding uncertainty in our annual carbon cycle assessments from 2003  
577 to 2007. Our results indicate that differences in simulated annual mean CO<sub>2</sub> exchanges

578 and NCB from climate sensitivity are greater than those from landscape heterogeneity  
579 (Figure 9a,c); i.e., annual CO<sub>2</sub> uptake strength is more sensitive to climate forcing  
580 uncertainty than to peatland type representation. In terms of the simulated annual mean  
581 CH<sub>4</sub> emissions and NGGB, our results indicate that variability from climate sensitivity is  
582 comparable to those from landscape heterogeneity (Figure 9b,d). Therefore, bias-  
583 corrected climate and realistic peatland characterization are both necessary to reduce the  
584 uncertainty in representing carbon cycling dynamics and their radiative forcing effects.

585 In addition to their effects on carbon cycle predictions, changes in climate  
586 conditions also affect permafrost degradation and thus induce changes in areal cover of  
587 peatland types. Malmer et al. (2005) showed that there were -0.95, 0.24, and 0.62 ha areal  
588 cover changes (-10.3%, 4.0%, and 46.3% percentage changes) from 1970 to 2000 in  
589 palsa, bog, and fen, respectively, at the Stordalen Mire. By applying the annual mean  
590 CO<sub>2</sub> and CH<sub>4</sub> exchanges simulated with bias-corrected climate from 2003 to 2007, the  
591 areal cover changes from 1970 to 2000 alone would lead to -44 kg C y<sup>-1</sup>, 76 kg C y<sup>-1</sup>, and  
592 2076 kg CO<sub>2</sub>-eq y<sup>-1</sup> changes in annual mean CO<sub>2</sub> exchanges, CH<sub>4</sub> exchanges, and NGGB,  
593 respectively, at the Stordalen Mire. The changes in landscape scale carbon cycle  
594 dynamics indicate that the radiative warming impact of increased CH<sub>4</sub> emissions is large  
595 enough to offset the radiative cooling impact of increased CO<sub>2</sub> uptake at the Stordalen  
596 Mire, consistent with the estimates reported in Deng et al. (2014). The areal cover  
597 changes across peatland types could persist or accelerate under the projected warming  
598 and wetting trends in the Arctic (Collins et al., 2013; Bintanja and Andry, 2017), which  
599 could stimulate CH<sub>4</sub> emissions and produce a stronger radiative warming impact.  
600

#### 601 **4. Conclusions**

602 We evaluated the climate bias in a widely used atmospheric reanalysis product  
603 (GSWP3) at our northern Sweden Stordalen Mire site. We then applied a comprehensive  
604 biogeochemistry model, *ecosys*, to estimate the effects of these biases on active layer  
605 development and carbon cycling across a thaw gradient at the site. Our results show that  
606 *ecosys* reasonably represented measured hydrological, thermal, and biogeochemical cycle  
607 processes in the intact permafrost palsa, partly thawed bog, and fen. We found that the  
608 cold and wet biases in the GSWP3 climate reanalysis dataset significantly alter model  
609 simulations, leading to biases in simulated Active Layer Depths, Net Carbon Balance,  
610 and Net Greenhouse Gas Balance by up to 28.6%, 38 g C m<sup>-2</sup> y<sup>-1</sup>, and 298 g CO<sub>2</sub>-eq m<sup>-2</sup>  
611 y<sup>-1</sup>, respectively. The Net Carbon Balance simulated with bias-corrected climate suggests  
612 that all the examined peatland types are currently net carbon sinks from the atmosphere,  
613 although the bog and fen sites can have positive radiative forcing impacts due to their  
614 higher CH<sub>4</sub> emissions.

615 Our results indicate that the annual means of ALD, CO<sub>2</sub> uptake, and CH<sub>4</sub>  
616 emissions generally increase along the permafrost thaw gradient at the Stordalen Mire  
617 under current climate, consistent with previous studies in this region. Our analysis  
618 suggests that palsa, bog, and fen differ strongly in their carbon cycling dynamics and  
619 have different responses to climate forcing biases. Differences in simulated CO<sub>2</sub> and CH<sub>4</sub>  
620 exchanges driven by uncertainty from climate forcing are as large as those from  
621 landscape heterogeneity across the examined permafrost thaw gradient. Model  
622 simulations demonstrate that the palsa site exhibits the strongest sensitivity to biases in  
623 air temperature and precipitation. The wet bias in GSWP3 could erroneously increase

624 predicted CH<sub>4</sub> emissions from the palsa site to a magnitude comparable to emissions  
625 currently measured in **the** bog and fen sites. These results also show that increased  
626 precipitation projected for high latitude regions could strongly accelerate CH<sub>4</sub> emissions  
627 from the palsa area, even without degradation of palsa into bog and fen. Future studies  
628 should thus recognize the effects of climate forcing uncertainty on carbon cycling, in  
629 addition to tracking changes in carbon budgets associated with areal changes in  
630 permafrost degradation.

631

### 632 **Acknowledgements**

633 This study was funded by the Genomic Science Program of the United States Department  
634 of Energy Office of Biological and Environmental Research under the ISOGENIE  
635 project, grant DE-SC0016440, to Lawrence Berkeley Laboratory under contract DE-  
636 AC02-05CH11231, and by support from the Swedish Research Council (VR) to PMC.  
637 We thank the Abisko Scientific Research Station of the Swedish Polar Research  
638 Secretariat for providing the meteorological data.

639

640 **References**

- 641 Ahlström, A., Schurgers, G. and Smith, B.: The large influence of climate model bias on  
642 terrestrial carbon cycle simulations, *Environmental Research Letters*, 12(1),  
643 014004, doi:[10.1088/1748-9326/12/1/014004](https://doi.org/10.1088/1748-9326/12/1/014004), 2017.
- 644 Anav, A., Friedlingstein, P., Kidston, M., Bopp, L., Ciais, P., Cox, P., Jones, C., Jung,  
645 M., Myneni, R. and Zhu, Z.: Evaluating the Land and Ocean Components of the  
646 Global Carbon Cycle in the CMIP5 Earth System Models, *J. Climate*, 26(18),  
647 6801–6843, doi:10.1175/JCLI-D-12-00417.1, 2013.
- 648 Arneth, A., Sitch, S., Pongratz, J., Stocker, B. D., Ciais, P., Poulter, B., Bayer, A. D.,  
649 Bondeau, A., Calle, L., Chini, L. P., Gasser, T., Fader, M., Friedlingstein, P.,  
650 Kato, E., Li, W., Lindeskog, M., Nabel, J. E. M. S., Pugh, T. A. M., Robertson,  
651 E., Viovy, N., Yue, C. and Zaehle, S.: Historical carbon dioxide emissions caused  
652 by land-use changes are possibly larger than assumed, *Nature Geoscience*, 10(2),  
653 79–84, doi:[10.1038/ngeo2882](https://doi.org/10.1038/ngeo2882), 2017.
- 654 Bäckstrand, K., Crill, P. M., Mastepanov, M., Christensen, T. R. and Bastviken, D.: Non-  
655 methane volatile organic compound flux from a subarctic mire in Northern  
656 Sweden, *Tellus B*, 60(2), 226–237, doi:[10.1111/j.1600-0889.2007.00331.x](https://doi.org/10.1111/j.1600-0889.2007.00331.x),  
657 2008a.
- 658 Bäckstrand, K., Crill, P. M., Mastepanov, M., Christensen, T. R. and Bastviken, D.: Total  
659 hydrocarbon flux dynamics at a subarctic mire in northern Sweden, *Journal of*  
660 *Geophysical Research: Biogeosciences*, 113(G3), doi:[10.1029/2008JG000703](https://doi.org/10.1029/2008JG000703),  
661 2008b.

662 Backstrand, K., Crill, P. M., ski, M. J.-K., Mastepanov, M., Christensen, T. R. and  
663 Bastviken, D.: Annual carbon gas budget for a subarctic peatland, Northern  
664 Sweden, 14, 2010.

665 Berrisford, P., Dee, D. P., Poli, P., Brugge, R., Fielding, K., Fuentes, M., Kållberg, P. W.,  
666 Kobayashi, S., Uppala, S. and Simmons, A.: The ERA-Interim archive Version  
667 2.0, 2011.

668 Bintanja, R. and Andry, O.: Towards a rain-dominated Arctic, Nature Climate Change,  
669 7(4), 263–267, doi:[10.1038/nclimate3240](https://doi.org/10.1038/nclimate3240), 2017.

670 Callaghan, T. V., Bergholm, F., Christensen, T. R., Jonasson, C., Kokfelt, U. and  
671 Johansson, M.: A new climate era in the sub-Arctic: Accelerating climate changes  
672 and multiple impacts, Geophysical Research Letters, 37(14),  
673 doi:[10.1029/2009GL042064](https://doi.org/10.1029/2009GL042064), 2010.

674 Chang, K.-Y., Paw U, K. T. and Chen, S.-H.: The importance of carbon-nitrogen  
675 biogeochemistry on water vapor and carbon fluxes as elucidated by a multiple  
676 canopy layer higher order closure land surface model, Agricultural and Forest  
677 Meteorology, 259, 60–74, doi:[10.1016/j.agrformet.2018.04.009](https://doi.org/10.1016/j.agrformet.2018.04.009), 2018.

678 Christensen, T. R., Johansson, T., Åkerman, H. J., Mastepanov, M., Malmer, N., Friborg,  
679 T., Crill, P. and Svensson, B. H.: Thawing sub-arctic permafrost: Effects on  
680 vegetation and methane emissions, Geophysical Research Letters, 31(4),  
681 doi:[10.1029/2003GL018680](https://doi.org/10.1029/2003GL018680), 2004.

682 Collins, M., R. Knutti, J. Arblaster, J.-L. Dufresne, T. Fichefet, P. Friedlingstein, X. Gao,  
683 W.J. Gutowski, T. Johns, G. Krinner, M. Shongwe, C. Tebaldi, A.J. Weaver and  
684 M. Wehner, 2013: Long-term Climate Change: Projections, Commitments and



685 Irreversibility. Climate Change 2013: The Physical Science Basis. Contribution of  
686 Working Group I to the Fifth Assessment Report of the Intergovernmental Panel  
687 on Climate Change. T. F. Stocker et al., Eds., Cambridge University Press, 1029-  
688 1136.

689 Compo, G. P., Whitaker, J. S., Sardeshmukh, P. D., Matsui, N., Allan, R. J., Yin, X.,  
690 Gleason, B. E., Vose, R. S., Rutledge, G., Bessemoulin, P., Brönnimann, S.,  
691 Brunet, M., Crouthamel, R. I., Grant, A. N., Groisman, P. Y., Jones, P. D., Kruk,  
692 M. C., Kruger, A. C., Marshall, G. J., Maugeri, M., Mok, H. Y., Nordli, Ø., Ross,  
693 T. F., Trigo, R. M., Wang, X. L., Woodruff, S. D. and Worley, S. J.: The  
694 Twentieth Century Reanalysis Project, Quarterly Journal of the Royal  
695 Meteorological Society, 137(654), 1–28, doi:[10.1002/qj.776](https://doi.org/10.1002/qj.776), 2011.

696 Cooper, M. D. A., Estop-Aragónés, C., Fisher, J. P., Thierry, A., Garnett, M. H.,  
697 Charman, D. J., Murton, J. B., Phoenix, G. K., Treharne, R., Kokelj, S. V., Wolfe,  
698 S. A., Lewkowicz, A. G., Williams, M. and Hartley, I. P.: Limited contribution of  
699 permafrost carbon to methane release from thawing peatlands, Nature Climate  
700 Change, 7(7), 507–511, doi:[10.1038/nclimate3328](https://doi.org/10.1038/nclimate3328), 2017.

701 Cox, P. M., Betts, R. A., Jones, C. D., Spall, S. A. and Totterdell, I. J.: Acceleration of  
702 global warming due to carbon-cycle feedbacks in a coupled climate model, 408,  
703 4, 2000.

704 Deng, J., Li, C., Frohling, S., Zhang, Y., Bäckstrand, K. and Crill, P.: Assessing effects of  
705 permafrost thaw on C fluxes based on multiyear modeling across a permafrost  
706 thaw gradient at Stordalen, Sweden, Biogeosciences, 11(17), 4753–4770,  
707 doi:[10.5194/bg-11-4753-2014](https://doi.org/10.5194/bg-11-4753-2014), 2014.

708 Dimitrov, D. D., Bhatti, J. S. and Grant, R. F.: The transition zones (ecotone) between  
709 boreal forests and peatlands: Ecological controls on ecosystem productivity along  
710 a transition zone between upland black spruce forest and a poor forested fen in  
711 central Saskatchewan, *Ecological Modelling*, 291, 96–108,  
712 doi:10.1016/j.ecolmodel.2014.07.020, 2014.

713 Dimitrov Dimitre D., Grant Robert F., Lafleur Peter M. and Humphreys Elyn R.:  
714 Modeling the effects of hydrology on gross primary productivity and net  
715 ecosystem productivity at Mer Bleue bog, *Journal of Geophysical Research:*  
716 *Biogeosciences*, 116(G4), doi:10.1029/2010JG001586, 2011.

717 Dirmeyer, P. A.: A History and Review of the Global Soil Wetness Project (GSWP),  
718 *Journal of Hydrometeorology*, 12(5), 729–749, doi:[10.1175/JHM-D-10-05010.1](https://doi.org/10.1175/JHM-D-10-05010.1),  
719 2011.

720 Friedlingstein, P., Cox, P., Betts, R., Bopp, L., von Bloh, W., Brovkin, V., Cadule, P.,  
721 Doney, S., Eby, M., Fung, I., Bala, G., John, J., Jones, C., Joos, F., Kato, T.,  
722 Kawamiya, M., Knorr, W., Lindsay, K., Matthews, H. D., Raddatz, T., Rayner, P.,  
723 Reick, C., Roeckner, E., Schnitzler, K.-G., Schnur, R., Strassmann, K., Weaver,  
724 A. J., Yoshikawa, C. and Zeng, N.: Climate–Carbon Cycle Feedback Analysis:  
725 Results from the C<sup>4</sup> MIP Model Intercomparison, *Journal of Climate*, 19(14),  
726 3337–3353, doi:[10.1175/JCLI3800.1](https://doi.org/10.1175/JCLI3800.1), 2006.

727 Friedlingstein, P., Meinshausen, M., Arora, V. K., Jones, C. D., Anav, A., Liddicoat, S.  
728 K. and Knutti, R.: Uncertainties in CMIP5 Climate Projections due to Carbon  
729 Cycle Feedbacks, *Journal of Climate*, 27(2), 511–526, doi:[10.1175/JCLI-D-12-  
730 00579.1](https://doi.org/10.1175/JCLI-D-12-00579.1), 2014.

731 Ghimire, B., Riley, W. J., Koven, C. D., Mu, M. and Randerson, J. T.: Representing leaf  
732 and root physiological traits in CLM improves global carbon and nitrogen cycling  
733 predictions, *Journal of Advances in Modeling Earth Systems*, 8(2), 598–613,  
734 doi:[10.1002/2015MS000538](https://doi.org/10.1002/2015MS000538), 2016.

735 Grant, R. F.: Modelling changes in nitrogen cycling to sustain increases in forest  
736 productivity under elevated atmospheric CO<sub>2</sub> and contrasting site conditions,  
737 *Biogeosciences*, 10(11), 7703–7721, doi:10.5194/bg-10-7703-2013, 2013.

738 Grant, R. F.: Nitrogen mineralization drives the response of forest productivity to soil  
739 warming: Modelling in ecosys vs. measurements from the Harvard soil heating  
740 experiment, *Ecological Modelling*, 288, 38–46,  
741 doi:10.1016/j.ecolmodel.2014.05.015, 2014.

742 Grant R. F. and Flanagan L. B.: Modeling stomatal and nonstomatal effects of water  
743 deficits on CO<sub>2</sub> fixation in a semiarid grassland, *Journal of Geophysical*  
744 *Research: Biogeosciences*, 112(G3), doi:10.1029/2006JG000302, 2007.

745 Grant, R. F. and Roulet, N. T.: Methane efflux from boreal wetlands: Theory and testing  
746 of the ecosystem model Ecosys with chamber and tower flux measurements,  
747 *Global Biogeochemical Cycles*, 16(4), 2-1-2–16, doi:10.1029/2001GB001702,  
748 2002.

749 Grant, R. F., Oechel, W. C. and Ping, C.-L.: Modelling carbon balances of coastal arctic  
750 tundra under changing climate, *Global Change Biology*, 9(1), 16–36,  
751 doi:10.1046/j.1365-2486.2003.00549.x, 2003.

752 Grant, R. F., Black, T. A., Humphreys, E. R. and Morgenstern, K.: Changes in net  
753 ecosystem productivity with forest age following clearcutting of a coastal

754 Douglas-fir forest: testing a mathematical model with eddy covariance  
755 measurements along a forest chronosequence, *Tree Physiol.*, 27(1), 115–131,  
756 2007a.

757 Grant, R. F., Arkebauer, T. J., Dobermann, A., Hubbard, K. G., Schimelfenig, T. T.,  
758 Suyker, A. E., Verma, S. B. and Walters, D. T.: Net Biome Productivity of  
759 Irrigated and Rainfed Maize–Soybean Rotations: Modeling vs. Measurements,  
760 *Agronomy Journal*, 99(6), 1404, doi:10.2134/agronj2006.0308, 2007b.

761 Grant, R. F., Barr, A. G., Black, T. A., Gaumont□Guay, D., Iwashita, H., Kidson, J.,  
762 McCAUGHEY, H., Morgenstern, K., Murayama, S., Nesic, Z., Saigusa, N.,  
763 Shashkov, A. and Zha, T.: Net ecosystem productivity of boreal jack pine stands  
764 regenerating from clearcutting under current and future climates, *Global Change*  
765 *Biology*, 13(7), 1423–1440, doi:10.1111/j.1365-2486.2007.01363.x, 2007c.

766 Grant, R. F., Margolis, H. A., Barr, A. G., Black, T. A., Dunn, A. L., Bernier, P. Y. and  
767 Bergeron, O.: Changes in net ecosystem productivity of boreal black spruce  
768 stands in response to changes in temperature at diurnal and seasonal time scales,  
769 *Tree Physiology*, 29(1), 1–17, doi:10.1093/treephys/tpn004, 2009a.

770 Grant, R. F., Barr, A. G., Black, T. A., Margolis, H. A., Dunn, A. L., Metsaranta, J.,  
771 Wang, S., McCaughey, J. H. and Bourque, C. A.: Interannual variation in net  
772 ecosystem productivity of Canadian forests as affected by regional weather  
773 patterns – A Fluxnet-Canada synthesis, *Agricultural and Forest Meteorology*,  
774 149(11), 2022–2039, doi:10.1016/j.agrformet.2009.07.010, 2009b.

775 Grant, R. F., Hutyyra, L. R., Oliveira, R. C., Munger, J. W., Saleska, S. R. and Wofsy, S.  
776 C.: Modeling the carbon balance of Amazonian rain forests: resolving ecological

777 controls on net ecosystem productivity, *Ecological Monographs*, 79(3), 445–463,  
778 doi:10.1890/08-0074.1, 2009c.

779 Grant, R. F., Barr, A. G., Black, T. A., Margolis, H. A., Mccaughey, J. H. and Trofymow,  
780 J. A.: Net ecosystem productivity of temperate and boreal forests after  
781 clearcutting—a Fluxnet-Canada measurement and modelling synthesis, *Tellus B:  
782 Chemical and Physical Meteorology*, 62(5), 475–496, doi:10.1111/j.1600-  
783 0889.2010.00500.x, 2010.

784 Grant, R. F., Kimball, B. A., Conley, M. M., White, J. W., Wall, G. W. and Ottman, M.  
785 J.: Controlled Warming Effects on Wheat Growth and Yield: Field Measurements  
786 and Modeling, *Agronomy Journal*, 103(6), 1742–1754,  
787 doi:10.2134/agronj2011.0158, 2011a.

788 Grant, R. F., Humphreys, E. R., Lafleur, P. M. and Dimitrov, D. D.: Ecological controls  
789 on net ecosystem productivity of a mesic arctic tundra under current and future  
790 climates, *Journal of Geophysical Research: Biogeosciences*, 116(G1),  
791 doi:10.1029/2010JG001555, 2011b.

792 Grant, R. F., Baldocchi, D. D. and Ma, S.: Ecological controls on net ecosystem  
793 productivity of a seasonally dry annual grassland under current and future  
794 climates: Modelling with ecosys, *Agricultural and Forest Meteorology*, 152, 189–  
795 200, doi:10.1016/j.agrformet.2011.09.012, 2012a.

796 Grant, R. F., Desai, A. R. and Sulman, B. N.: Modelling contrasting responses of wetland  
797 productivity to changes in water table depth, *Biogeosciences*, 9(11), 4215–4231,  
798 doi:10.5194/bg-9-4215-2012, 2012b.

799 Grant R. F., Humphreys E. R. and Lafleur P. M.: Ecosystem CO<sub>2</sub> and CH<sub>4</sub> exchange in a  
800 mixed tundra and a fen within a hydrologically diverse Arctic landscape: 1.  
801 Modeling versus measurements, *Journal of Geophysical Research:*  
802 *Biogeosciences*, 120(7), 1366–1387, doi:10.1002/2014JG002888, 2015.

803 Grant, R. F., Mekonnen, Z. A., Riley, W. J., Wainwright, H. M., Graham, D. and Torn,  
804 M. S.: Mathematical Modelling of Arctic Polygonal Tundra with Ecosys: 1.  
805 Microtopography Determines How Active Layer Depths Respond to Changes in  
806 Temperature and Precipitation, *Journal of Geophysical Research: Biogeosciences*,  
807 122(12), 3161–3173, doi:[10.1002/2017JG004035](https://doi.org/10.1002/2017JG004035), 2017a.

808 Grant, R. F., Mekonnen, Z. A., Riley, W. J., Arora, B. and Torn, M. S.: Mathematical  
809 Modelling of Arctic Polygonal Tundra with *Ecosys*: 2. Microtopography  
810 Determines How CO<sub>2</sub> and CH<sub>4</sub> Exchange Responds to Changes in Temperature  
811 and Precipitation: GHG Exchange in Arctic Polygonal Tundra, *Journal of*  
812 *Geophysical Research: Biogeosciences*, 122(12), 3174–3187,  
813 doi:[10.1002/2017JG004037](https://doi.org/10.1002/2017JG004037), 2017b.

814 Guo, D., Wang, H. and Wang, A.: Sensitivity of Historical Simulation of the Permafrost  
815 to Different Atmospheric Forcing Data Sets from 1979 to 2009, *Journal of*  
816 *Geophysical Research: Atmospheres*, 122(22), 12,269–12,284,  
817 doi:[10.1002/2017JD027477](https://doi.org/10.1002/2017JD027477), 2017.

818 Harris, I., Jones, P. D., Osborn, T. J. and Lister, D. H.: Updated high-resolution grids of  
819 monthly climatic observations – the CRU TS3.10 Dataset, *International Journal of*  
820 *Climatology*, 34(3), 623–642, doi:10.1002/joc.3711, n.d.

821 Hodgkins, S. B., Tfaily, M. M., McCalley, C. K., Logan, T. A., Crill, P. M., Saleska, S.  
822 R., Rich, V. I. and Chanton, J. P.: Changes in peat chemistry associated with  
823 permafrost thaw increase greenhouse gas production, Proceedings of the National  
824 Academy of Sciences, 111(16), 5819–5824, doi:[10.1073/pnas.1314641111](https://doi.org/10.1073/pnas.1314641111), 2014.

825 van den Hurk, B., Kim, H., Krinner, G., Seneviratne, S. I., Derksen, C., Oki, T., Douville,  
826 H., Colin, J., Ducharne, A., Cheruy, F., Viovy, N., Puma, M. J., Wada, Y., Li, W.,  
827 Jia, B., Alessandri, A., Lawrence, D. M., Weedon, G. P., Ellis, R., Hagemann, S.,  
828 Mao, J., Flanner, M. G., Zampieri, M., Matera, S., Law, R. M. and Sheffield, J.:  
829 LS3MIP (v1.0) contribution to CMIP6: the Land Surface, Snow and Soil moisture  
830 Model Intercomparison Project – aims, setup and expected outcome,  
831 Geoscientific Model Development, 9(8), 2809–2832, doi:10.5194/gmd-9-2809-  
832 2016, 2016.

833 Hugelius, G., Strauss, J., Zubrzycki, S., Harden, J. W., Schuur, E. A. G., Ping, C.-L.,  
834 Schirrmeister, L., Grosse, G., Michaelson, G. J., Koven, C. D.,  
835 O&apos;Donnell, J. A., Elberling, B., Mishra, U., Camill, P., Yu, Z.,  
836 Palmtag, J. and Kuhry, P.: Estimated stocks of circumpolar permafrost carbon  
837 with quantified uncertainty ranges and identified data gaps, Biogeosciences,  
838 11(23), 6573–6593, doi:10.5194/bg-11-6573-2014, 2014.

839 IPCC, 2014: Climate Change 2014: Synthesis Report. Contribution of Working Groups I,  
840 II and III to the Fifth Assessment Report of the Intergovernmental Panel on  
841 Climate Change [Core Writing Team, R.K. Pachauri and L.A. Meyer (eds.)].  
842 IPCC, Geneva, Switzerland, 151 pp.

843 Johansson, M., Callaghan, T. V., Bosiö, J., Åkerman, H. J., Jackowicz-Korczynski, M.  
844 and Christensen, T. R.: Rapid responses of permafrost and vegetation to  
845 experimentally increased snow cover in sub-arctic Sweden, *Environmental*  
846 *Research Letters*, 8(3), 035025, doi:[10.1088/1748-9326/8/3/035025](https://doi.org/10.1088/1748-9326/8/3/035025), 2013.

847 Johansson, T., Malmer, N., Crill, P. M., Friborg, T., Åkerman, J. H., Mastepanov, M. and  
848 Christensen, T. R.: Decadal vegetation changes in a northern peatland, greenhouse  
849 gas fluxes and net radiative forcing, *Global Change Biology*, 12(12), 2352–2369,  
850 doi:[10.1111/j.1365-2486.2006.01267.x](https://doi.org/10.1111/j.1365-2486.2006.01267.x), 2006.

851 Jones, M. C., Harden, J., O'Donnell, J., Manies, K., Jorgenson, T., Treat, C. and Ewing,  
852 S.: Rapid carbon loss and slow recovery following permafrost thaw in boreal  
853 peatlands, *Glob. Chang. Biol.*, 23(3), 1109–1127, doi:[10.1111/gcb.13403](https://doi.org/10.1111/gcb.13403), 2017.

854 Kalnay, E., Kanamitsu, M., Kistler, R., Collins, W., Deaven, D., Gandin, L., Iredell, M.,  
855 Saha, S., White, G., Woollen, J., Zhu, Y., Chelliah, M., Ebisuzaki, W., Higgins,  
856 W., Janowiak, J., Mo, K. C., Ropelewski, C., Wang, J., Leetmaa, A., Reynolds,  
857 R., Jenne, R. and Joseph, D.: The NCEP/NCAR 40-Year Reanalysis Project, *Bull.*  
858 *Amer. Meteor. Soc.*, 77(3), 437–472, doi:[10.1175/1520-0477\(1996\)077<0437:TNYRP>2.0.CO;2](https://doi.org/10.1175/1520-0477(1996)077<0437:TNYRP>2.0.CO;2), 1996.

860 Kanamitsu, M., Ebisuzaki, W., Woollen, J., Yang, S.-K., Hnilo, J. J., Fiorino, M. and  
861 Potter, G. L.: NCEP–DOE AMIP-II Reanalysis (R-2), *Bull. Amer. Meteor. Soc.*,  
862 83(11), 1631–1644, doi:[10.1175/BAMS-83-11-1631](https://doi.org/10.1175/BAMS-83-11-1631), 2002.

863 Kokfelt, U., Reuss, N., Struyf, E., Sonesson, M., Rundgren, M., Skog, G., Rosen, P., and  
864 Hammarlund, D.: Wetland development, permafrost history and nutrient cycling



865 inferred from late Holocene peat and lake sediment records in subarctic Sweden,  
866 *J. Paleolimn.*, 44, 327–342, doi:10.1007/s10933-010-9406-8, 2010.

867 Lundin, E. J., Klaminder, J., Giesler, R., Persson, A., Olefeldt, D., Heliasz, M.,  
868 Christensen, T. R. and Karlsson, J.: Is the subarctic landscape still a carbon sink?  
869 Evidence from a detailed catchment balance, *Geophysical Research Letters*,  
870 43(5), 1988–1995, doi:[10.1002/2015GL066970](https://doi.org/10.1002/2015GL066970), 2016.

871 Malmer, N., Johansson, T., Olsrud, M. and Christensen, T. R.: Vegetation, climatic  
872 changes and net carbon sequestration in a North-Scandinavian subarctic mire over  
873 30 years, *Global Change Biology*, 11(11), 1895–1909, doi:[10.1111/j.1365-](https://doi.org/10.1111/j.1365-2486.2005.01042.x)  
874 [2486.2005.01042.x](https://doi.org/10.1111/j.1365-2486.2005.01042.x), 2005.

875 Mastepanov, M., Sigsgaard, C., Dlugokencky, E. J., Houweling, S., Ström, L., Tamstorf,  
876 M. P. and Christensen, T. R.: Large tundra methane burst during onset of  
877 freezing, *Nature*, 456(7222), 628–630, doi:[10.1038/nature07464](https://doi.org/10.1038/nature07464), 2008.

878 McCalley, C. K., Woodcroft, B. J., Hodgkins, S. B., Wehr, R. A., Kim, E.-H., Mondav,  
879 R., Crill, P. M., Chanton, J. P., Rich, V. I., Tyson, G. W. and Saleska, S. R.:  
880 Methane dynamics regulated by microbial community response to permafrost  
881 thaw, *Nature*, 514(7523), 478–481, doi:[10.1038/nature13798](https://doi.org/10.1038/nature13798), 2014.

882 Mezbahuddin, M., Grant, R. F. and Hirano, T.: Modelling effects of seasonal variation in  
883 water table depth on net ecosystem CO<sub>2</sub> exchange of a tropical peatland,  
884 *Biogeosciences*, 11(3), 577–599, doi:[10.5194/bg-11-577-2014](https://doi.org/10.5194/bg-11-577-2014), 2014.

885 Mondav, R., McCalley, C. K., Hodgkins, S. B., Frohling, S., Saleska, S. R., Rich, V. I.,  
886 Chanton, J. P. and Crill, P. M.: Microbial network, phylogenetic diversity and  
887 community membership in the active layer across a permafrost thaw gradient,

888 Environmental Microbiology, 19(8), 3201–3218, doi:[10.1111/1462-2920.13809](https://doi.org/10.1111/1462-2920.13809),  
889 2017.

890 Mondav, R., Woodcroft, B. J., Kim, E.-H., McCalley, C. K., Hodgkins, S. B., Crill, P.  
891 M., Chanton, J., Hurst, G. B., VerBerkmoes, N. C., Saleska, S. R., Hugenholtz, P.,  
892 Rich, V. I. and Tyson, G. W.: Discovery of a novel methanogen prevalent in  
893 thawing permafrost, Nature Communications, 5, 3212, doi:[10.1038/ncomms4212](https://doi.org/10.1038/ncomms4212),  
894 2014.

895 Myhre, G., D. Shindell, F.-M. Bréon, W. Collins, J. Fuglestedt, J. Huang, D. Koch, J.-F.  
896 Lamarque, D. Lee, B. Mendoza, T. Nakajima, A. Robock, G. Stephens, T.  
897 Takemura and H. Zhang, 2013: Anthropogenic and Natural Radiative Forcing. In:  
898 Climate Change 2013: The Physical Science Basis. Contribution of Working  
899 Group I to the Fifth Assessment Report of the Intergovernmental Panel on  
900 Climate Change [Stocker, T.F., D. Qin, G.-K. Plattner, M. Tignor, S.K. Allen, J.  
901 Boschung, A. Nauels, Y. Xia, V. Bex and P.M. Midgley (eds.)]. Cambridge  
902 University Press, Cambridge, United Kingdom and New York, NY, USA, pp.  
903 659–740, doi:10.1017/CBO9781107415324.018.

904 O'Donnell, J. A., Jorgenson, M. T., Harden, J. W., McGuire, A. D., Kanevskiy, M. Z. and  
905 Wickland, K. P.: The Effects of Permafrost Thaw on Soil Hydrologic, Thermal,  
906 and Carbon Dynamics in an Alaskan Peatland, Ecosystems, 15(2), 213–229,  
907 doi:10.1007/s10021-011-9504-0, 2012.

908 Olefeldt, D. and Roulet, N. T.: Effects of permafrost and hydrology on the composition  
909 and transport of dissolved organic carbon in a subarctic peatland complex, Journal

910 of Geophysical Research: Biogeosciences, 117(G1), doi:[10.1029/2011JG001819](https://doi.org/10.1029/2011JG001819),  
911 2012.

912 Piao, S., Liu, Z., Wang, T., Peng, S., Ciais, P., Huang, M., Ahlstrom, A., Burkhardt, J. F.,  
913 Chevallier, F., Janssens, I. A., Jeong, S.-J., Lin, X., Mao, J., Miller, J.,  
914 Mohammat, A., Myneni, R. B., Peñuelas, J., Shi, X., Stohl, A., Yao, Y., Zhu, Z.  
915 and Tans, P. P.: Weakening temperature control on the interannual variations of  
916 spring carbon uptake across northern lands, *Nature Climate Change*, 7(5), 359–  
917 363, doi:[10.1038/nclimate3277](https://doi.org/10.1038/nclimate3277), 2017.

918 Raz-Yaseef, N., Torn, M. S., Wu, Y., Billesbach, D. P., Liljedahl, A. K., Kneafsey, T. J.,  
919 Romanovsky, V. E., Cook, D. R. and Wullschleger, S. D.: Large CO<sub>2</sub> and CH<sub>4</sub>  
920 emissions from polygonal tundra during spring thaw in northern Alaska,  
921 *Geophysical Research Letters*, 44(1), 504–513, doi:[10.1002/2016GL071220](https://doi.org/10.1002/2016GL071220),  
922 2017.

923 Rydén, B. E., Fors, L. and Kostov, L.: Physical Properties of the Tundra Soil-Water  
924 System at Stordalen, Abisko, *Ecological Bulletins*, (30), 27–54, 1980.

925 Rydén B. E. and Kostov, L.: Thawing and freezing in tundra soil. In: *Ecology of a*  
926 *Subarctic Mire, Ecological Bulletins, Vol. 30 (ed. Sonesson M), pp. 251–282.*  
927 *Swedish Natural Science Research Council, Stockholm, 1980.*

928 Schuur, E. a. G., McGuire, A. D., Schädel, C., Grosse, G., Harden, J. W., Hayes, D. J.,  
929 Hugelius, G., Koven, C. D., Kuhry, P., Lawrence, D. M., Natali, S. M., Olefeldt,  
930 D., Romanovsky, V. E., Schaefer, K., Turetsky, M. R., Treat, C. C. and Vonk, J.  
931 E.: Climate change and the permafrost carbon feedback, *Nature*, 520(7546), 171–  
932 179, doi:[10.1038/nature14338](https://doi.org/10.1038/nature14338), 2015.

933 Sonesson, M. (1972) Cryptogams. In: International biological programme—Swedish  
934 tundra biome project. Technical report No. 9, April 1972. Swedish Natural  
935 Science Research Council Ecological Research Committee.

936 Tokida, T., Miyazaki, T., Mizoguchi, M., Nagata, O., Takakai, F., Kagemoto, A. and  
937 Hatano, R.: Falling atmospheric pressure as a trigger for methane ebullition from  
938 peatland, *Global Biogeochemical Cycles*, 21(2), doi:10.1029/2006GB002790,  
939 2007.

940 Viovy, N.: CRUNCEP Version 7 - Atmospheric Forcing Data for the Community Land  
941 Model, Research Data Archive at the National Center for Atmospheric Research,  
942 Computational and Information Systems Laboratory, Boulder CO.

943 Wickland, K. P., Striegl, R. G., Neff, J. C. and Sachs, T.: Effects of permafrost melting  
944 on CO<sub>2</sub> and CH<sub>4</sub> exchange of a poorly drained black spruce lowland, *Journal of*  
945 *Geophysical Research: Biogeosciences*, 111(G2), doi:[10.1029/2005JG000099](https://doi.org/10.1029/2005JG000099),  
946 2006.

947 Woodcroft, B. J., Singleton, C. M., Boyd, J. A., Evans, P. N., Emerson, J. B., Zayed, A.  
948 A. F., Hoelzle, R. D., Lamberton, T. O., McCalley, C. K., Hodgkins, S. B.,  
949 Wilson, R. M., Purvine, S. O., Nicora, C. D., Li, C., Frohking, S., Chanton, J. P.,  
950 Crill, P. M., Saleska, S. R., Rich, V. I. and Tyson, G. W.: Genome-centric view of  
951 carbon processing in thawing permafrost, *Nature*, doi:[10.1038/s41586-018-0338-](https://doi.org/10.1038/s41586-018-0338-1)  
952 [1](https://doi.org/10.1038/s41586-018-0338-1), 2018.

953 Wu, Z., Ahlström, A., Smith, B., Ardö, J., Eklundh, L., Fensholt, R. and Lehsten, V.:  
954 Climate data induced uncertainty in model-based estimations of terrestrial

955 primary productivity, Environmental Research Letters, 12(6), 064013,  
956 doi:10.1088/1748-9326/aa6fd8, 2017.

957 Yoshimura, K. and Kanamitsu, M.: Dynamical Global Downscaling of Global  
958 Reanalysis, Monthly Weather Review, 136(8), 2983–2998,  
959 doi:[10.1175/2008MWR2281.1](https://doi.org/10.1175/2008MWR2281.1), 2008.

960 Zaehle, S., Friend, A. D., Friedlingstein, P., Dentener, F., Peylin, P. and Schulz, M.:  
961 Carbon and nitrogen cycle dynamics in the O-CN land surface model: 2. Role of  
962 the nitrogen cycle in the historical terrestrial carbon balance, Global  
963 Biogeochemical Cycles, 24(1), doi:[10.1029/2009GB003522](https://doi.org/10.1029/2009GB003522), 2010.

964 Zimov, S. A., Davydov, S. P., Zimova, G. M., Davydova, A. I., Schuur, E. a. G., Dutta,  
965 K. and Chapin, F. S.: Permafrost carbon: Stock and decomposability of a globally  
966 significant carbon pool, Geophysical Research Letters, 33(20),  
967 doi:[10.1029/2006GL027484](https://doi.org/10.1029/2006GL027484), 2006.

968

969 Table 1. Temporal coverage of quality-controlled CO<sub>2</sub> and CH<sub>4</sub> exchanges measured by  
 970 automated chambers at the three peatland types in the Stordalen Mire during the years  
 971 2002 to 2007.

Sites	Number of data points	CO <sub>2</sub>		Number of data points	CH <sub>4</sub>	
		3 Hourly coverage (%)	Daily coverage (%)		3 Hourly coverage (%)	Daily coverage (%)
Palsa	12752	65.8	12.4	N/A	N/A	N/A
Bog	12821	68.5	12.7	6660	96.2	25.0
Fen	8989	63.8	13.7	4923	90.5	33.7

972 The temporal coverage represents the percentage of data points that are passed our  
 973 quality-controlled threshold at the corresponding time steps.

974 Table 2. Evaluation of the 3 hourly and daily CO<sub>2</sub> and CH<sub>4</sub> exchanges simulated at the  
 975 palsa, bog, and fen sites.

Sites	C component	3-Hourly		Daily	
		R <sup>2</sup>	RRMSEs (%)	R <sup>2</sup>	RRMSEs (%)
Palsa	CO <sub>2</sub>	0.48	13.4	0.36	18.3
Bog	CO <sub>2</sub>	0.63	19.1	0.44	35.8
	CH <sub>4</sub>	0.31	16.3	0.47	22.3
Fen	CO <sub>2</sub>	0.64	8.4	0.43	25.5
	CH <sub>4</sub>	0.44	11.1	0.54	16.9

976 RRMSEs are relative root mean squared errors.

977

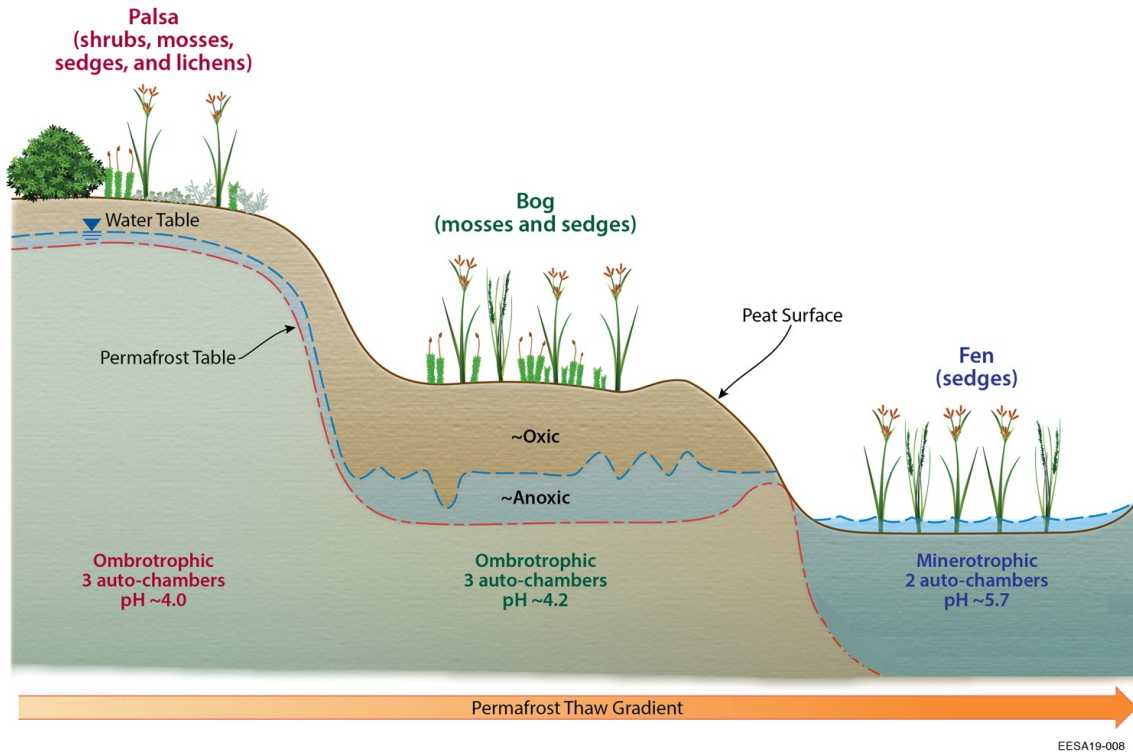
978 Table 3. Means and standard deviations of cumulative CO<sub>2</sub> and CH<sub>4</sub> exchanges simulated  
 979 in the palsa, bog, and fen during the period 2003 to 2007.

Sites	C flux component	Growing season; Days 119–288		Non-growing season; Days 1–118 and 289–365	
		Mean	Standard deviation	Mean	Standard deviation
Palsa	CO <sub>2</sub>	-72.70	19.10	38.89	4.09
	CH <sub>4</sub>	0.04	0.02	0.01	0.002
Bog	CO <sub>2</sub>	-79.59	21.46	42.89	2.16
	CH <sub>4</sub>	3.52	0.45	0.42	0.11
Fen	CO <sub>2</sub>	-88.65	7.26	44.41	6.13
	CH <sub>4</sub>	10.86	3.95	0.78	0.18

980 All gas exchanges are in units of g C m<sup>-2</sup>.

981





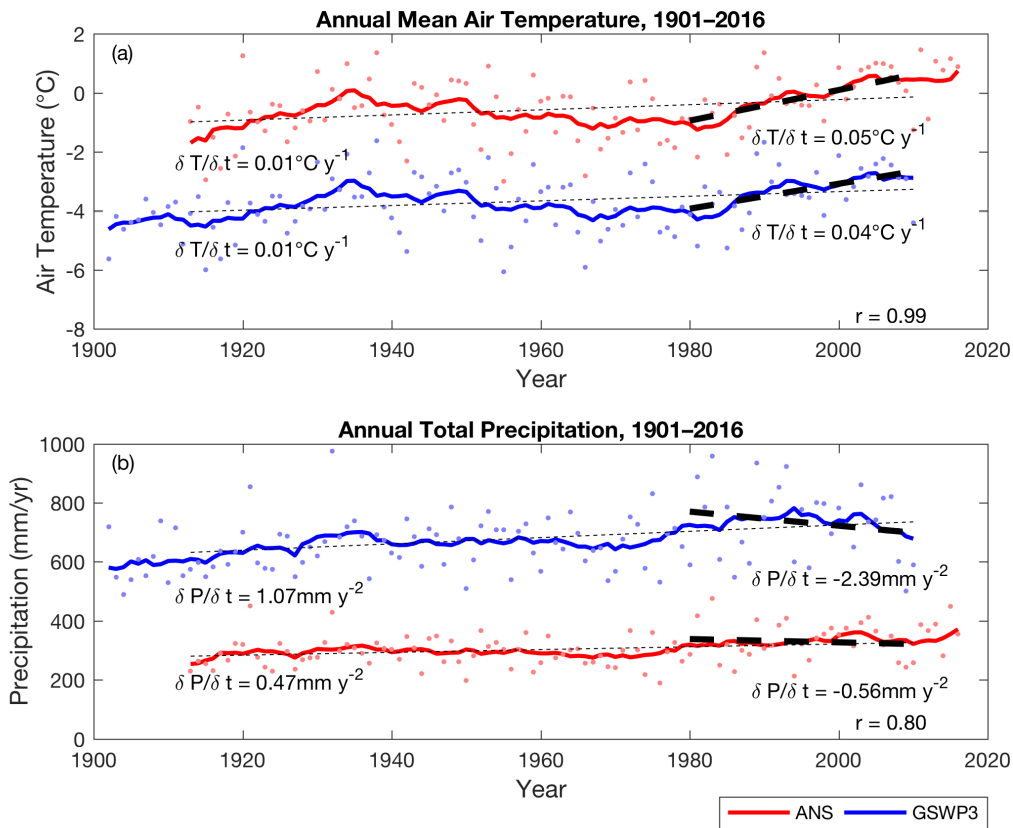
EESA19-008

982

983 Figure 1. Schematic diagram of the sampling sites at Stordalen Mire, adapted from

984 Johansson et al. (2006).

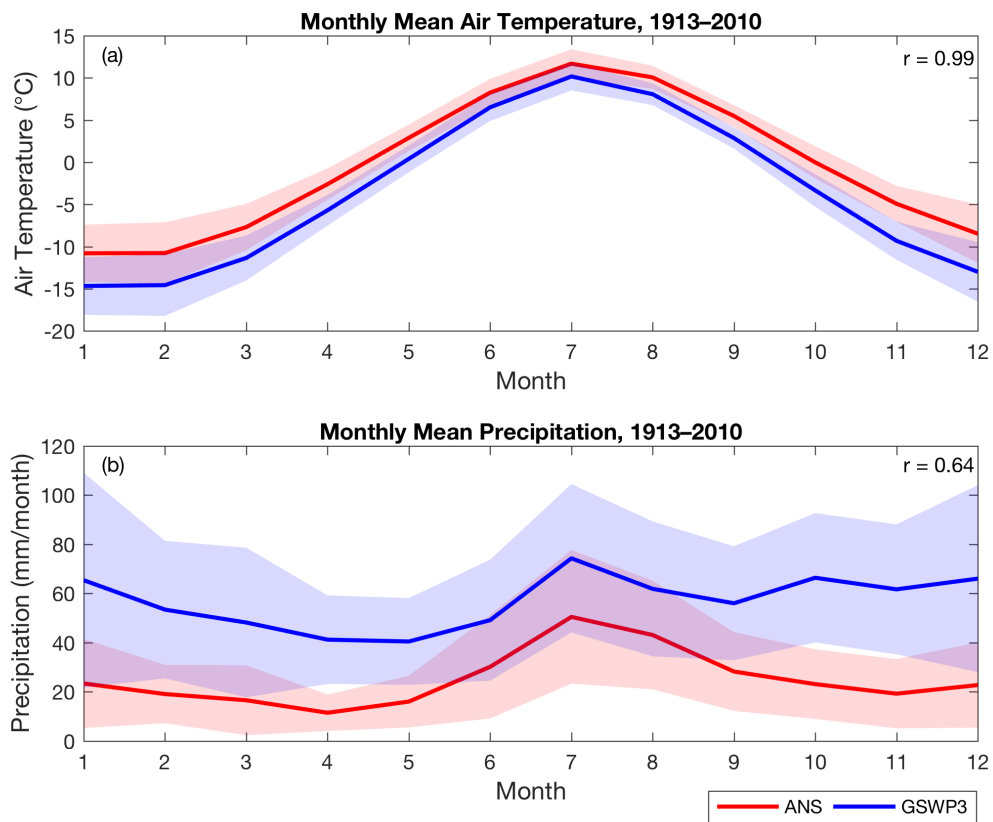
985



986

987 Figure 2. Time series of air temperature (a) and precipitation (b) measured at ANS (red;  
 988 years 1913–2016) and extracted from GSWP3 (blue; years 1901–2010). Dots are the  
 989 annual means and solid lines are the decadal moving averages of the corresponding  
 990 annual means. Thin and thick dashed lines are the trends for years 1913–2010, and years  
 991 1980–2010, respectively. The inset  $r$  values are the correlation coefficients calculated  
 992 between the two time series.

993

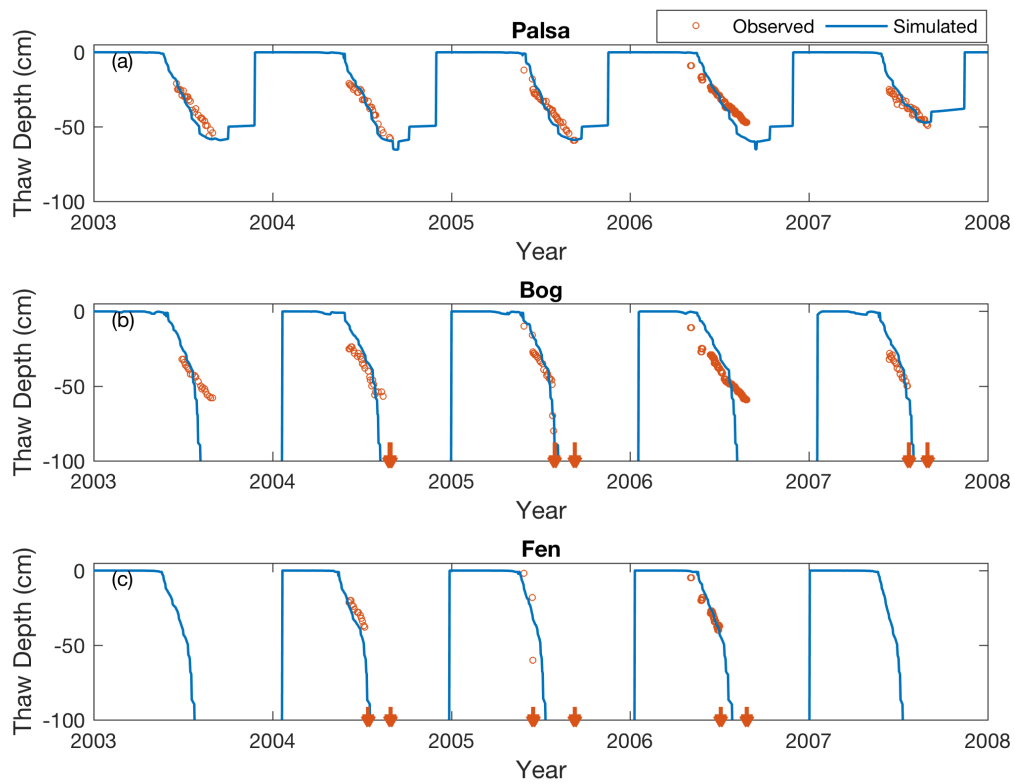


994

995 Figure 3. Monthly mean air temperature (a) and precipitation (b) measured at ANS (red)  
 996 and extracted from GSWP3 (blue). The shaded area is the inter-annual variability for the  
 997 corresponding dataset, represented by the standard deviations calculated at each month.

998 The inset  $r$  values are the correlation coefficients calculated between the two time series.

999



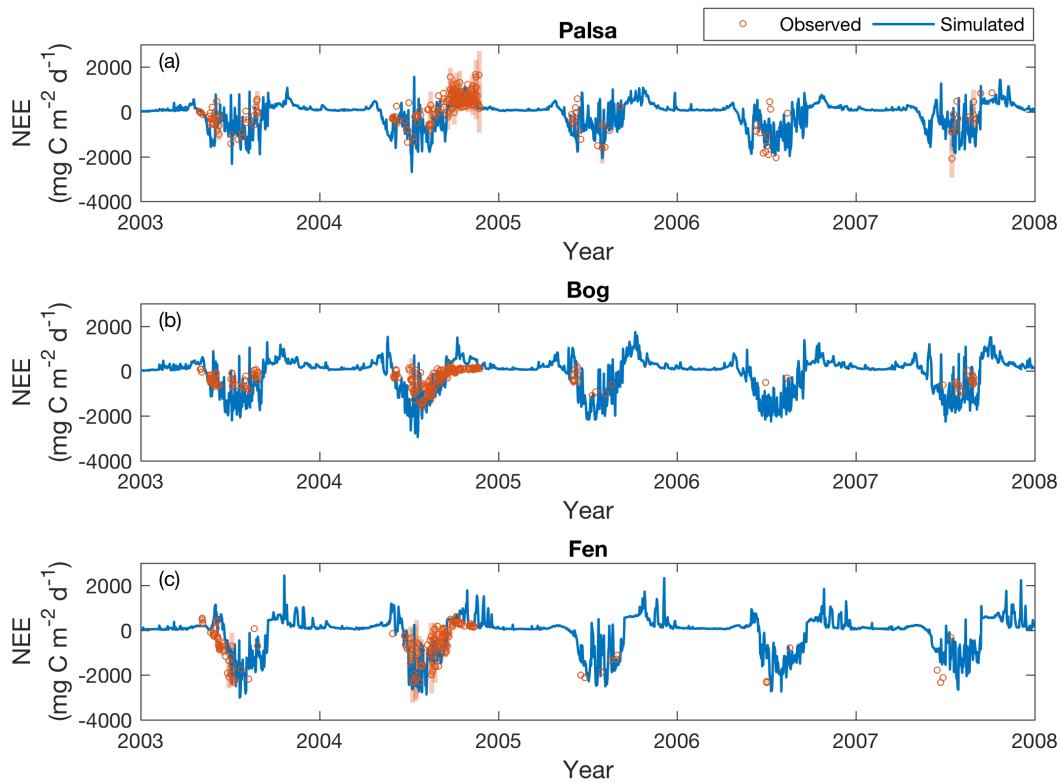
1000

1001 Figure 4. Simulated (solid lines) and measured (open circles) seasonal dynamics of thaw

1002 depth at the palsa (a), bog (b), and fen (c) sites from 2003 to 2007. Downward arrows

1003 indicate the time when measured thaw depth exceeds 90 cm for a measurement year.

1004



1005

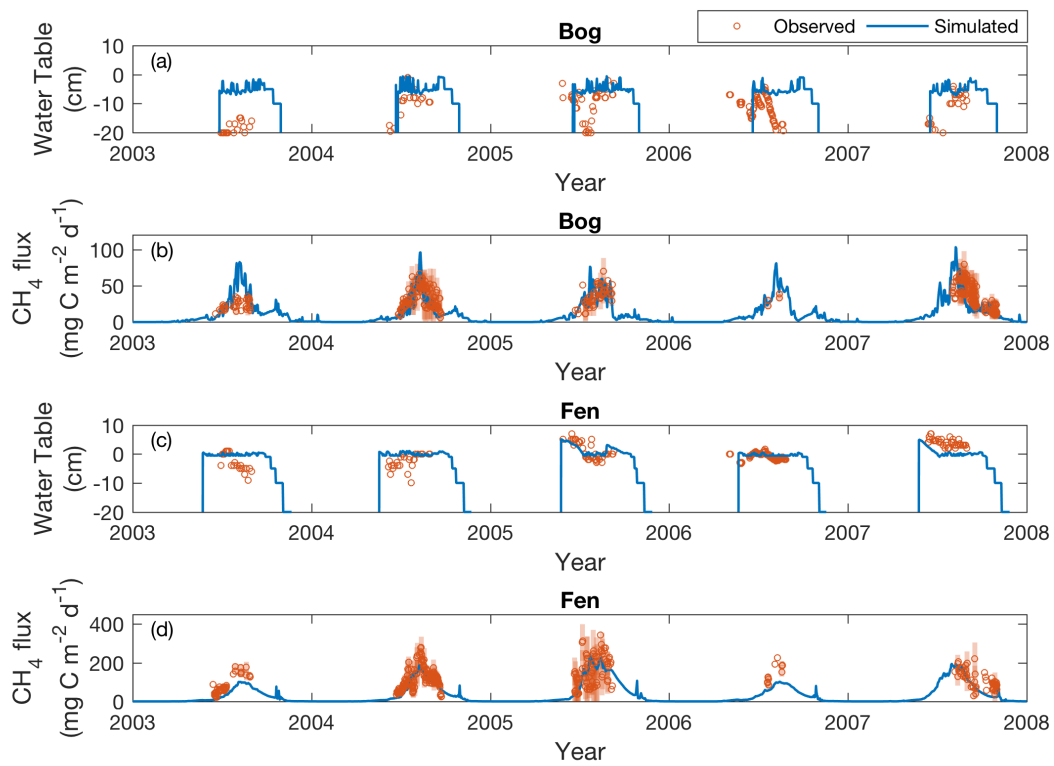
1006 Figure 5. Simulated (solid lines) and measured (open circles) daily CO<sub>2</sub> exchanges (NEE)

1007 at the palsa (a), bog (b), and fen (c) sites, from 2003 to 2007. Shaded bars are the

1008 standard deviations of daily NEE measured across subsites under each peatland type.

1009 Positive and negative values indicate effluxes from and influxes to the site, respectively.

1010



1011

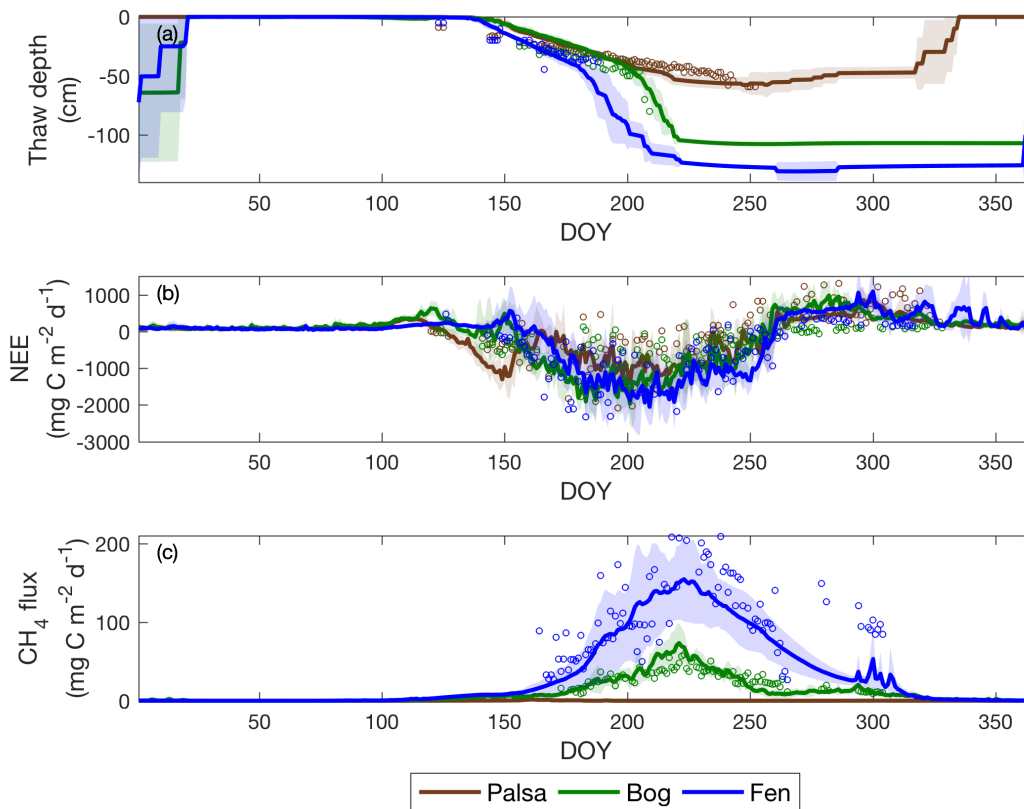
1012 Figure 6. Simulated (solid lines) and measured (open circles) water table depths

1013 CH<sub>4</sub> emissions at the bog and fen from 2003 to 2007. Shaded bars are the standard

1014 deviations of the daily CH<sub>4</sub> emissions measured across the subsites under each peatland

1015 type.

1016



1017

1018 Figure 7. Daily thaw depth (a), daily NEE (b), and daily CH<sub>4</sub> (c) exchanges for the three

1019 sites from 2003 to 2007. Solid lines and open circles are the simulated and measured

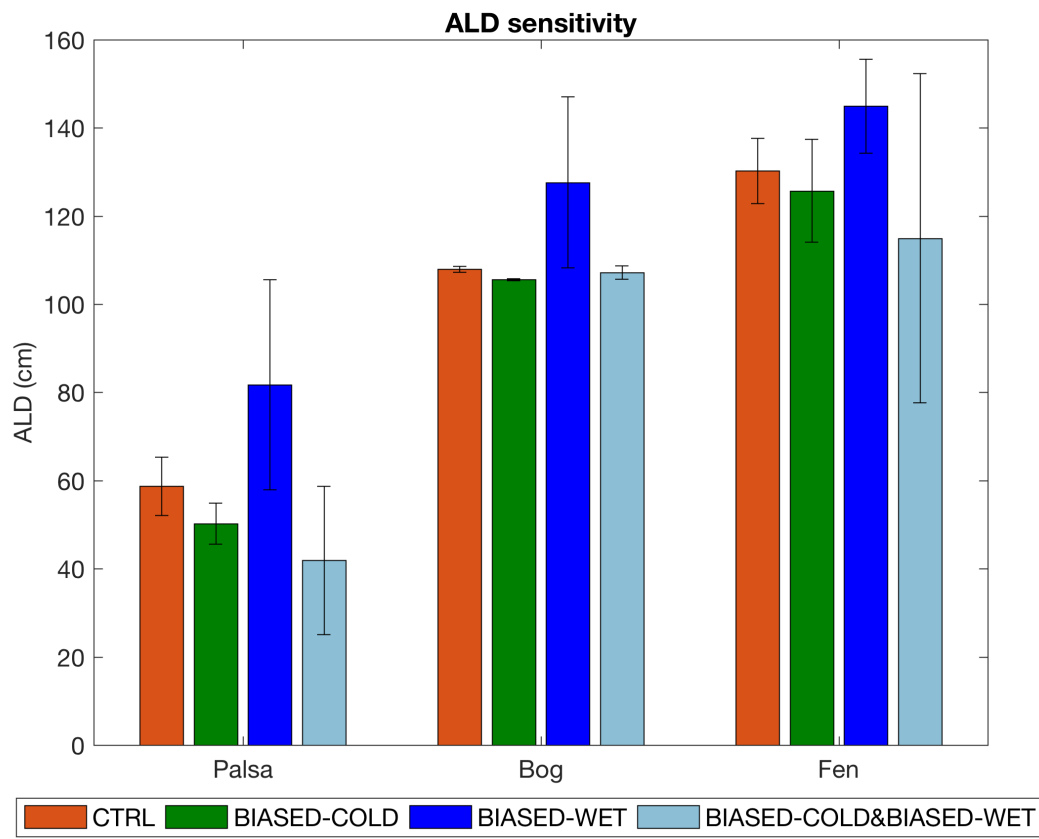
1020 inter-annual means for each day of year, respectively. The shaded area is the simulated

1021 inter-annual variability for the corresponding dataset, represented by the standard

1022 deviations calculated at each day of year. Positive and negative carbon flux values

1023 indicate effluxes from and influxes to the site, respectively.

1024



1025

1026

Figure 8. Simulated ALD at the palsa, bog, and fen for four sets of climate forcing

1027

(Section 2.5). Bars and error bars are means and standard deviations calculated from

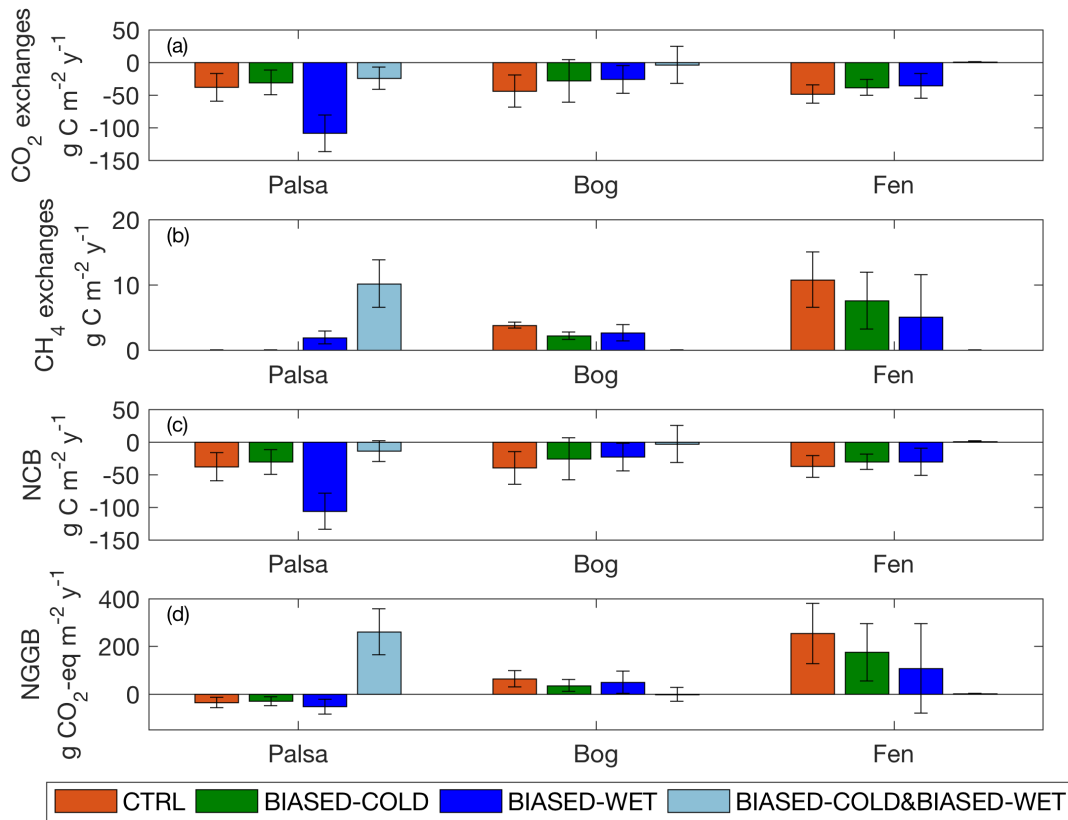
1028

2003 to 2007, respectively.

1029

1030





1031

1032 Figure 9. Annual CO<sub>2</sub> exchanges (a), CH<sub>4</sub> exchanges (b), Net Carbon Balance (c), and  
 1033 Net Greenhouse Gas Balance (d) simulated at the palsa, bog, and fen, under each set of  
 1034 simulations. Bars and error bars are the means and standard deviations calculated from  
 1035 2003 to 2007, respectively. Positive and negative values indicate effluxes from and  
 1036 influxes to the site, respectively.

1037

1038